AN ANALYSIS OF THE VARIATION OF OCEAN FLOOR BATHYMETRY AND HEAT FLOW WITH AGE

Barry Parsons and John G. Sclater

Department of Earth and Planetary Sciences, Massachusetts Institute of Technology
Cambridge, Massachusetts 02139

Abstract. Two models, a simple cooling model and the plate model, have been advanced to account for the variation in depth and heat flow with increasing age of the ocean floor. The simple cooling model predicts a linear relation between depth and $t^{\frac{1}{2}}$, and heat flow and $1/t^{\frac{1}{2}}$, where t is the age of the ocean floor. We show that the same $t^{\frac{1}{2}}$ dependence is implicit in the solutions for the plate model for sufficiently young ocean floor. For larger ages these relations break down, and depth and heat flow decay exponentially to constant values. The two forms of the solution are developed to provide a simple method of inverting the data to give the model parameters. The empirical depth versus age relation for the North Pacific and North Atlantic has been extended out to 160 m.y. B.P. The depth initially increases as $t^{\frac{1}{2}}$, but between 60 and 80 m.y. B.P. the variation of depth with age departs from this simple relation. For older ocean floor the depth decays exponentially with age toward a constant asymptotic value. Such characteristics would be produced by a thermal structure close to that of the plate model. Inverting the data gives a plate thickness of 125±10 km, a bottom boundary temperature of 1350°±275°C, and a thermal expansion coefficient of $(3.2\pm1.1) \times 10^{-5}°C^{-1}$. Between 0 and 70 m.y. B.P. the depth can be represented by the relation $d(t) = 2500 + 350t^{\frac{1}{2}}$ m, with t in m.y. B.P., and for regions older than 20 m.y. B.P. by the relation $d(t) = 6400 - 3200 \exp(-t/62.8)$ m. The heat flow data were treated in a similar, but less extensive manner. Although the data are compatible with the same model that accounts for the topography, their scatter prevents their use in the same quantitative fashion. Our analysis shows that the heat flow only responds to the bottom boundary at approximately twice the age at which the depth does. Within the scatter of the data, from 0 to 120 m.y. B.P., the heat flow can be represented by the relation $q(t) = 11.3/t^{\frac{1}{2}}$ μcal cm^{-2} s^{-1}. The previously accepted view that the heat flow observations approach a constant asymptotic value in the old ocean basins needs to be tested more stringently. The above results imply that a mechanism is required to supply heat at the base of the plate.

Introduction

The broad features of ocean floor heat flow and topography are generally accepted to be explicable within the framework of plate tectonics. Both are the result of the cooling of hot material after it has accreted to the plate near a midocean ridge and moves away as part of the plate. It has been less clear whether the cooling alone can account for the way the heat flow and the mean depth vary with age of the oceanic plate. If, in addition, a source of heat at the base of the plate is required, this would provide a constraint on convection in the upper mantle. In order to establish whether this is necessary or not we propose to reexamine the variation of bathymetry and heat flow with age, in particular, for older ocean floor.

In the original idea of Holmes [1931], as revived by Hess [1962], midocean ridges were the surface expressions of the ascending limb of a convection cell in the mantle. Turcotte and Oxburgh [1967] examined this model quantitatively by means of an asymptotic boundary layer treatment of cellular convection. The variation of heat flow calculated from their model was found to show rough agreement with the observations. McKenzie [1967], however, following a model suggested by Langseth et al. [1966], found an alternative explanation in the cooling of a rigid plate moving at constant velocity away from a hot boundary at the ridge crest. The plate was assumed to have a constant thickness in order to reproduce the approximately constant heat flux background observed in the older ocean basins. This model also produced rough agreement with the heat flow data and was later shown to be capable of explaining the variation in depth away from the midocean ridges [Vogt and Ostenso, 1967; McKenzie and Sclater, 1969; Sleep, 1969]. Because the amount of cooling depends on time, it soon became clear that a more meaningful presentation of the data was in terms of the age of the ocean floor rather than distance away from the ridge crest. In this manner, Sclater and Francheteau [1970] and Sclater et al. [1971] showed that there were empirical relationships between heat flow and age, and depth and age, that were similar for all oceans. The empirical curves could be reproduced with fair agreement by the plate model, given a suitable choice of parameters.

There are, however, inconsistent or incomplete features about this model. One is that the thickness of the slab is arbitrarily prescribed and there is no physical mechanism that determines it. Second, the heat flux at the ridge crest and, in fact, the integrated heat flux are infinite. To overcome these limitations, Sorokhtin [1973] and Parker and Oldenburg [1973] proposed an alternative model. Here the bottom boundary of the lithosphere was taken to be the solid-liquid phase boundary of the material. A boundary condition was chosen in which the heat

Paper number 6B0585.

removed by the plate at the ridge crest balances the heat of solidification and cooling in a zone of intrusion at this boundary. This model has a lithosphere whose thickness is everywhere determined by the physical parameters of the system, and the choice of boundary condition removes the singularity in the integrated heat flux. In fact, in the original McKenzie [1967] model the singularity in heat flux at the ridge crest can be removed in a similar way by changing the boundary condition on the vertical boundary [Davis and Lister, 1974; Lubimova and Nikitina, 1975]. Parker and Oldenburg [1973] found that, except very near the ridge crest, the thickness of the plate increased as $t^{\frac{1}{2}}$, where t is the age of the plate. Consequently, in their model the heat flow will vary asymptotically as $t^{-\frac{1}{2}}$, and the depth increases linearly as $t^{\frac{1}{2}}$.

Subsequent to this, Davis and Lister [1974], after an analysis of the one-dimensional heat flow equation, plotted the original topographic data of Sclater et al. [1971] against $t^{\frac{1}{2}}$ and found a good linear relationship within the age range of the data (0-80 m.y.). As we shall see, the $t^{\frac{1}{2}}$ dependence is a property of all thermal models of ridge crests, at least in a limited age range. Most comparisons with data had been made by using the model of McKenzie [1967], the solution for which contains no hint of any $t^{\frac{1}{2}}$ structure. In fact, this has to be implicit in the solution, however well disguised, and we have reformulated the solution to make the $t^{\frac{1}{2}}$ dependence explicit. Together the two different forms of the solution provide a useful new way of characterizing the data.

If the heat flow and depth continued indefinitely to vary as $t^{-\frac{1}{2}}$ and $t^{\frac{1}{2}}$, respectively, it would be possible to explain all the heat lost at the ocean floor by cooling of a lithospheric boundary layer. Heat flow measurements in older ocean floor had suggested an approach to a constant value, which was the original rationale for the plate model. This, in turn, requires a supply of heat (about 1 μcal cm^{-2} s^{-1}) at the base of the plate, providing an important constraint in discussing mantle convection. Such a constraint has been used in a recently proposed scheme in which convection in the mantle occurs on two distinct horizontal length scales [Richter, 1973; Richter and Parsons, 1975; McKenzie and Weiss, 1975]. The motion of the plates and the associated return flow form one component termed the large-scale flow. Small-scale convection, analogous to the forms of convection in fluid layers that have been studied so extensively, is postulated in order to supply the assumed background heat flux at the base of the plate. Such a two-scale system exhibits a wide variety of convective features and provides a potential explanation for a correspondingly wide variety of features on the earth's surface [Richter and Parsons, 1975; McKenzie and Weiss, 1975]. If the heat flow does in fact approach a background level, one would expect the depth also to tend to constant value, and this would provide additional support for the arguments used in the above scheme.

These considerations form the background to this paper. All models of the thermal structure of the lithosphere [Turcotte and Oxburgh, 1967; McKenzie, 1967; Parker and Oldenburg, 1973] are basically solutions of the equation of heat transport. They differ in the assumptions made as to the nature of the boundary layer and hence in the boundary conditions that are applied. However, the different solutions should all possess those features determined by the structure of the equations. In section 2 and the appendices we show how the solution of McKenzie [1967] can be reconstructed to make explicit the $t^{\frac{1}{2}}$ dependence possessed by the other two models. This analysis also suggests how the data can be simply characterized. Section 3 therefore is concerned with a reexamination of ocean floor heat flow and depth from this point of view. Measurements of the depth plotted by Davis and Lister [1974] were in the age range 0-80 m.y. Here this range is extended out to 160 m.y. B.P. by using average depths calculated from suites of topographic profiles in the North Pacific and North Atlantic oceans. The variation of heat flow is reexamined by using heat flow averages in given age zones in the manner of Sclater and Francheteau [1970]. These are supplemented by averages calculated in an attempt to provide more reliable heat flow averages [Sclater et al., 1976].

From this we observe the simple $t^{\frac{1}{2}}$ dependence for the depth in the age range 0-70 m.y. At this age the curve departs from the linear relationship in the manner that would be expected for a lithospheric plate of a given thickness, as had been suggested by the preliminary studies of Sclater et al. [1975] and Morgan [1975]. Asymptotic relations that describe the observed variation of depth and heat flow with age are given. The values of the constants defined in section 2 are obtained from fits to the data; these are then used to estimate physical properties of the lithosphere such as its thickness, the bottom boundary temperature, and thermal expansion coefficient and to give estimates of the errors in these quantities. Finally, we discuss the possible uncertainties in the analysis and interpretation of the data.

Methods of Characterizing the Data

The properties of solutions for the thermal structure of a moving slab are presented here in order to explain the various ways of plotting the data that are made use of in the next section. The geometry of the problem, as originally formulated by McKenzie [1967], is shown in Figure 1. If a steady state is assumed and internal heat generation neglected, then the temperature is governed by the time independent equation of heat transport,

$$\underline{v} \cdot \underline{\nabla} T = \kappa \nabla^2 T \qquad (1)$$

where $\underline{v}$ is the velocity of the slab, T is the temperature, and κ is the thermal diffusivity. The thermal diffusivity is given by $\kappa = k/\rho C_p$, k being the thermal conductivity, ρ the density, and C_p the specific heat. Equation (1) can be nondimensionalized by using the following expressions

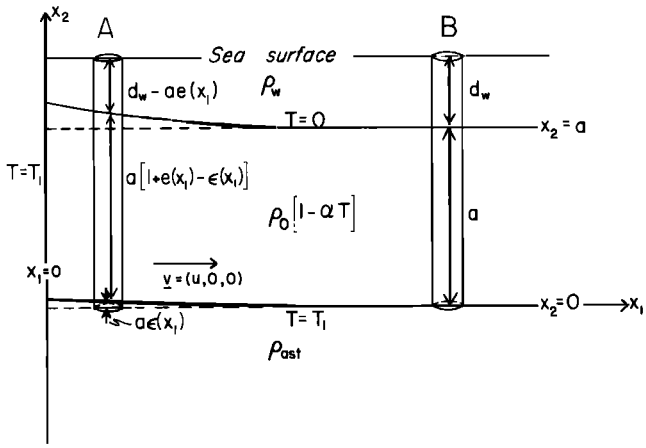

Fig. 1. Sketch showing the geometry and boundary conditions of the plate model and the method of calculating the elevation. Columns A and B of equal cross-sectional area must have equal masses above a common level $x_2 = 0$. This gives

$$\rho_w d_w + \int_0^a \rho_o[1 - \alpha T(\infty, x_2)]\, dx_2 = \rho_w[d - ae(x_1)] + \int_{a\varepsilon(x_1)}^{a[1+\rho(x_1)]} \rho_o[1 - \alpha T(x_1, x_2)]\, dx_2 + \rho_{ast}\, a\varepsilon(x_1)$$

where α is the thermal expansion coefficient, ρ_w the density of seawater, ρ_o the density of the lithosphere at 0°C, ρ_{ast} the asthenospheric density, d_w the asymptotic depth at large distance from the ridge crest, $ae(x_1)$ the elevation of the ridge, and $a\varepsilon(x_1)$ the displacement of the bottom of the lithosphere above the level of compensation.

$$\begin{aligned} T &= T_1 T' \\ x_1 &= a x_1' \\ x_2 &= a x_2' \end{aligned} \qquad (2)$$

Substitution in (1) gives

$$\frac{\partial^2 T}{\partial x_1^2} - 2R\frac{\partial T}{\partial x_1} + \frac{\partial^2 T}{\partial x_2^2} = 0 \qquad (3)$$

where we have immediately dropped the primes on the nondimensional variables. The nondimensional parameter

$$R = ua/2\kappa \qquad (4)$$

is the thermal Reynolds number for this problem, or as it is generally known, the Peclet number. The solution which satisfies the boundary conditions shown in Figure 1 and remains bounded for large values of x_1 has the form

$$T = (1 - x_2) + \sum_{n=1}^{\infty} a_n \sin n\pi x_2 \exp(-\beta_n x_1) \qquad (5)$$

with

$$\beta_n = [(R^2 + n^2\pi^2)^{1/2} - R]$$

and

$$a_n = \frac{2(-1)^{n+1}}{n\pi}$$

A feature of this solution noted above is that the surface heat flux and the integrated surface heat flux diverge at $x_1 = 0$ due to the singular boundary condition there.

A simplification that is often used comes from neglecting the horizontal conduction term relative to the convective term in (3). This then reduces to

$$\partial T/\partial t = \partial^2 T/\partial x_2^2 \qquad (6)$$

the one-dimensional heat flow equation, where a nondimensional form for time $t = x_1/2R$ has been used. The solution of this equivalent one-dimensional problem is discussed in Appendix 1. There it is shown that one can find a solution which displays an explicit dependence on $t^{1/2}$ not apparent in the solution corresponding to (5). In Appendix 2 we show that, by using a Green's function approach, a form of solution to the full equation (3) can be found which reduces asymptotically away from the ridge crest to the solution of (6), which displays the explicit $t^{1/2}$ dependence. Furthermore, when $x_1/2R \ll 1$, which is equivalent using dimensioned quantities to $\kappa t \ll a^2$, this solution behaves asymptotically as

$$T \sim \text{erf}\left[\frac{1 - x_2}{2(t)^{1/2}}\right] \qquad (7)$$

This is the solution for the cooling of an infinite half space that Davis and Lister [1974] used in their justification of the plots against $t^{1/2}$. We see therefore that at small times the same property is possessed by a slab of finite thickness, and so in this age range it should also have the resulting properties of a depth that varies linearly with $t^{1/2}$ and heat flow varying as $t^{-1/2}$.

Means for deriving expressions for heat flow and topography are given in the work by Sclater and Francheteau [1970]. The dimensional surface heat flux, derived using (5), is

$$-k\left[\frac{\partial T}{\partial x_2}\right]_{x_2=a} = \frac{kT_1}{a} \cdot \left\{1 + 2\sum_{n=1}^{\infty} \exp[(R - (R^2 + n^2\pi^2)^{1/2})x_1']\right\} \qquad (8)$$

where x_1' is the nondimensional distance, the prime being restored as we shall now use both dimensional and nondimensional variables. The topography is calculated in the fashion illustrated in Figure 1. If the temperature solution $T(x_1, x_2)$ from (5) is used, to first order in α, the elevation is

$$e(x_1') = \frac{4\alpha\rho_o T_1}{(\rho_o - \rho_w)\pi^2} \sum_{k=0}^{\infty} \left\{ \frac{1}{(2k+1)^2} \cdot \exp\left[[R - (R^2 + (2k+1)^2\pi^2)^{1/2}]x_1' \right] \right\} \quad (9)$$

where we have taken the asthenospheric density $\rho_{ast} \approx \rho_o$ and $\rho_{ast}\, \varepsilon(x_1) = \rho_w e(x_1)$. The expression for the elevation has contributions only from terms with odd n in (5), as terms with even n leave the mean density of the slab unchanged and thus do not disturb the overall equilibrium.

We can also obtain alternative expressions in the same way which will hold when $\kappa t^{\frac{1}{2}} << a$ by using the asymptotic solution (7). The surface heat flux, written as a function of age, is then

$$-k \left(\frac{\partial T}{\partial x_2}\right)_{x_2=a} = \rho_o C_p T_1 \left(\frac{\kappa}{\pi t}\right)^{1/2} \quad (10)$$

so that the heat flow varies as $t^{-\frac{1}{2}}$ for small enough ages. The asymptotic expression (7) can be used instead of (5) to obtain an expression for the topography

$$ae(t) = \frac{\rho_o a\alpha T_1}{2(\rho_o - \rho_w)} - \frac{2\rho_o \alpha T_1}{(\rho_o - \rho_w)} \left(\frac{\kappa t}{\pi}\right)^{1/2} \quad (11)$$

valid when $(\kappa t)^{\frac{1}{2}} << a$.

For young ocean floor then the plate model predicts that the ocean floor depth should increase as $t^{\frac{1}{2}}$. The model also predicts that in older ocean floor the depth should become constant, as can be seen from (9). Hence if the depth is plotted as a function of $t^{\frac{1}{2}}$, initially we should see a straight line whose slope is given in (11), and eventually the curve should break away from this line and tend steadily to a constant value. In Figure 2a the elevation is plotted versus the square root of x_1' for different values of R. The curves have the form described, and this kind of plot forms the basis of the first way of characterizing the data. First of all we note that

$$x_1'/2R = \kappa t/a^2 \quad (12)$$

which is then recognizable as the usual non-dimensional form of time. Also when $R >> n\pi$, the exponent in (5) is approximately

$$[(R^2 + n^2\pi^2)^{1/2} - R]x_1' \simeq n^2\pi^2(x_1'/2R) \quad (13)$$

Thus if the elevation or heat flow is plotted against some function of $x_1'/2R$ the result is independent of R except very close to the ridge crest, where the higher n terms make their most important contribution. For spreading rates greater than 1 cm/yr, as $R > 25$, this approximation holds well and means that only one plot is necessary rather than several for different values of R. An illustration of this is given in Figure 2b. For each R an estimate is made of the value of $(x_1')^{\frac{1}{2}}$ for which the elevation departs by a constant fraction (5%) from the straight line. These values are plotted against $2R^{\frac{1}{2}}$ in Figure 2b, and the results show a linear relationship. The slope of this line gives the particular value of $(x_1'/2R)^{\frac{1}{2}}$ at which the linear relation between elevation and $t^{\frac{1}{2}}$ breaks down, and this is given by

$$x_1'/2R \sim 0.11 \quad (14)$$

which is close to a relationship of the form

$$\kappa t/a^2 \sim 1/\pi^2 \quad (15)$$

which might be expected from the form of solution (24) in Appendix 1. If the age at which this occurs can be estimated in the data, (14) would provide a relationship between κ and a. The occurrence of such a break in a plot of depth versus $t^{\frac{1}{2}}$ would also be proof of the influence of some bottom boundary condition.

The heat flow should demonstrate a similar initial linear relationship if it is plotted against $(x_1'/2R)^{-\frac{1}{2}}$ with a subsequent approach to a constant asymptotic value. Unfortunately, a property of such a plot is to distort considerably the horizontal scale of $x_1'/2R$ in the range where the heat flux background approaches the constant background value. This makes it difficult to determine where the curve departs from a linear relationship. Instead, in Figure 3 we have plotted heat flow, given by (8), against $(x_1'/2R)$ on logarithmic scales, so that the simple relationship appears as a straight line with a slope of -1/2. The curve departs from a linear relationship at a nondimensional age approximately twice that given by (14). Hence the depth is a more sensitive indicator of the influence of a bottom boundary condition. This is because the elevation is an integrated effect through the slab, whereas the heat flow depends only on the thermal structure close to the surface.

The simple asymptotic relationships for small t have therefore suggested ways of plotting the data which will enable us to extract directly characteristic numbers relating the lithospheric parameters, e.g., relation (15). There is yet another way of plotting the data which comes from considering the asymptotic forms for large t and is given by the form of the original solution (5). It can be clearly seen that for large t the elevation will follow an asymptotic relation given by

$$\log_{10}[ae(t)] \sim \log_{10} \frac{4\alpha a\rho_o T_1}{(\rho_o - \rho_w)\pi^2} - \frac{\pi^2\kappa(\log_{10} e)t}{a^2} \quad (16)$$

remembering that $R >> \pi$, as other terms decay more rapidly. The heat flow exhibits a similar relationship. From (8), for large t we would expect

$$\log_{10}\left[q - \frac{kT_1}{a}\right] \sim \log_{10} \frac{2kT_1}{a} - \frac{\pi^2\kappa(\log_{10} e)t}{a^2} \quad (17)$$

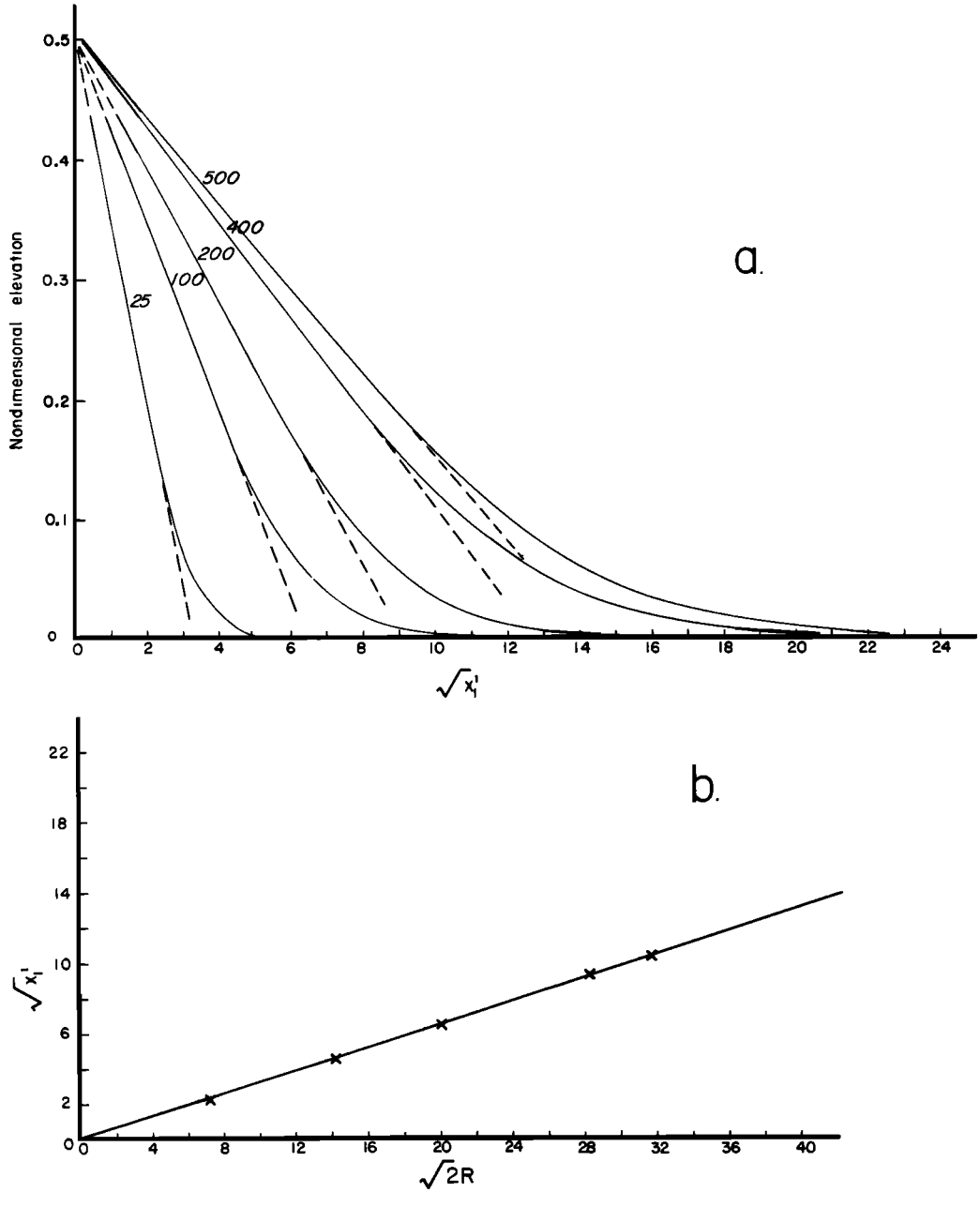

Fig. 2. (a) Plot of nondimensional elevation for the plate model versus the square root of the nondimensional distance for various values of the thermal Reynolds number R. The dashed lines near the origin indicate where there are very small departures from the linear relation for small values of R. All the lines intersect at a common point for $x_1' = 0$. (b) The value of $(x_1')^{\frac{1}{2}}$ at which the elevation departs from the linear relationship by more than 5% plotted versus $(2R)^{\frac{1}{2}}$.

where q is the heat flux and the heat flow anomaly is measured relative to the asymptotic constant background level kT_1/a. Expressions (16) and (17) suggest that the logarithm of the elevation or heat flow anomaly should be plotted versus age. In Figure 4a the elevation calculated from the full expression (9) has been plotted on a logarithmic scale versus age. The curve approaches a linear relationship very rapidly indeed. The logarithm of the heat flow anomaly approaches a linear relationship with age but less quickly than it does for the elevation (Figure 4b). This is because terms with n even are missing from the expression for the elevation, as was explained above, and the second term decays much more rapidly than the second term in the heat flow expression. The linear expression for the $\log_{10}[e(t)]$ versus t plots holds for values of $\kappa t/a^2 > 0.025$, which overlaps considerably with the linear $t^{\frac{1}{2}}$ relationship.

To make these plots in practice involves an assumption, which turns out to be quite reasonable. In using the $t^{\frac{1}{2}}$ plots one can consider depth rather than elevation and obtain essentially the same relationship. However, in order to plot the elevation as in (16) or heat

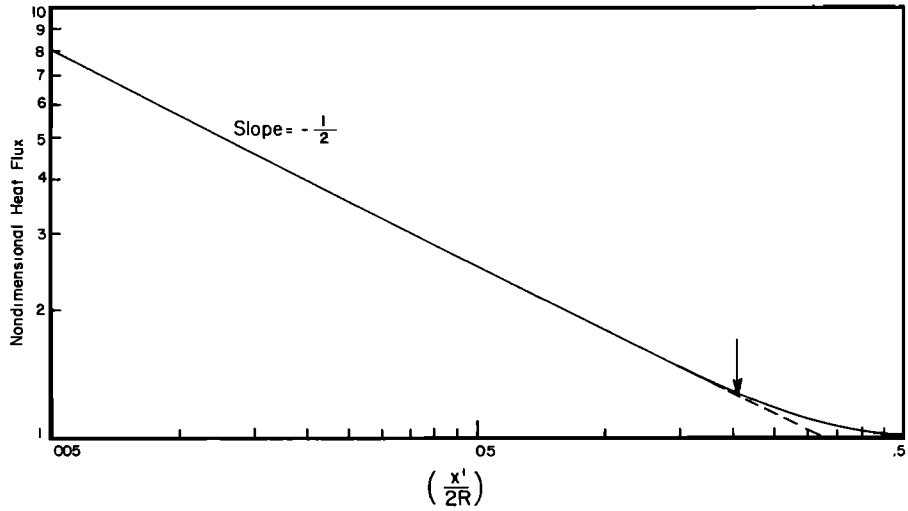

Fig. 3. Nondimensional heat flow on a logarithmic scale plotted versus (x'/2R) also on a logarithmic scale. The linear relation with respect to $t^{-\frac{1}{2}}$ appears as a straight line with a slope of -1/2. The age at which this relationship breaks down is marked by the arrow and is approximately twice the equivalent age for the elevation.

flow anomaly as in (17) it must be assumed that we know the asymptotic constant values toward which the depth and heat flow tend. The maximum age of the ocean floor is limited, but the greatest age for which we have depth data is more than twice the age at which the plot of depth versus $t^{\frac{1}{2}}$ departs from a linear relationship. This value is given by (15), and consideration of (9) or (16) then implies that at this deepest value more than 9/10 of the original elevation has decayed. Hence by using an initial estimate for the time constant $a^2/\pi^2\kappa$ the reference depth can be evaluated from the depth in the oldest part of the oceans. The same considerations apply to estimating the heat flow anomaly.

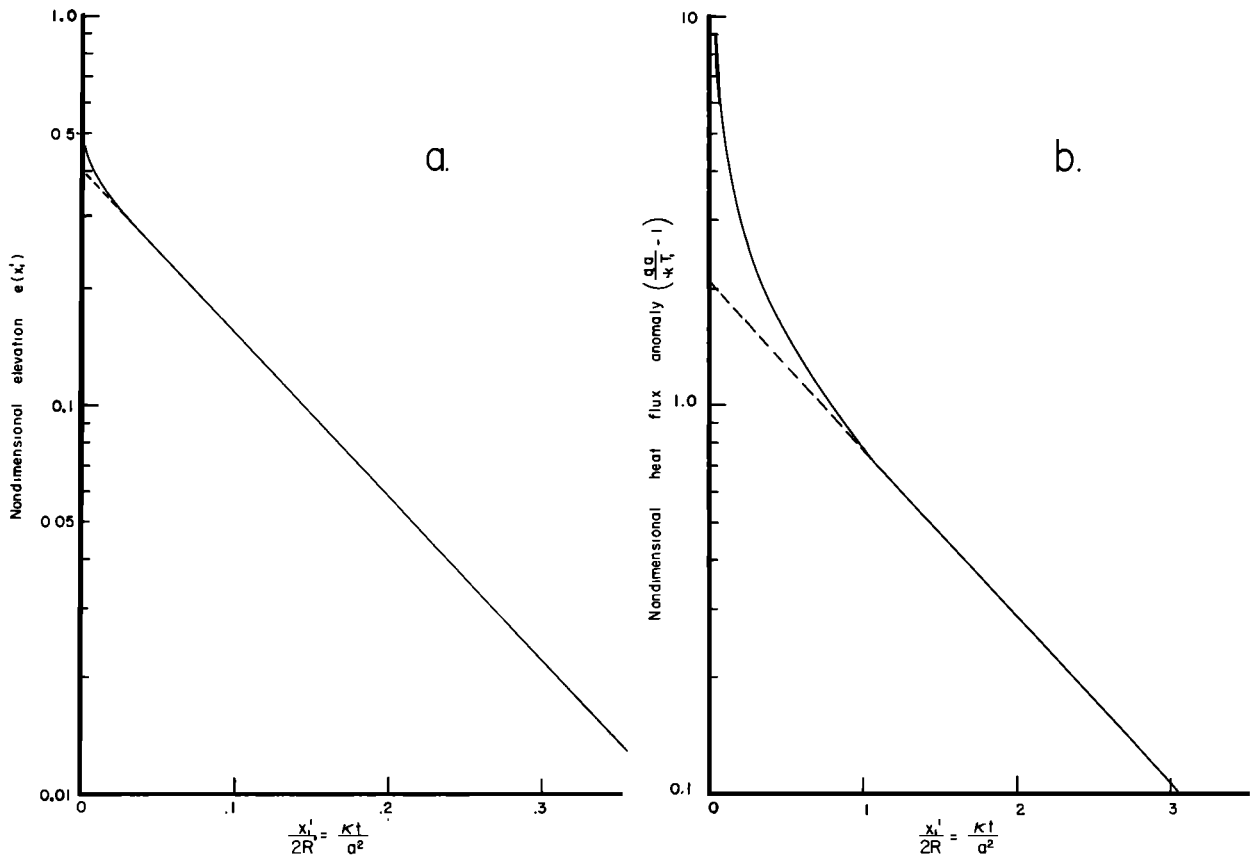

Fig. 4. (a) Nondimensional elevation on a logarithmic scale versus nondimensional time. (b) The nondimensional heat flux anomaly measured relative to the uniform background plotted on a logarithmic scale versus nondimensional time.

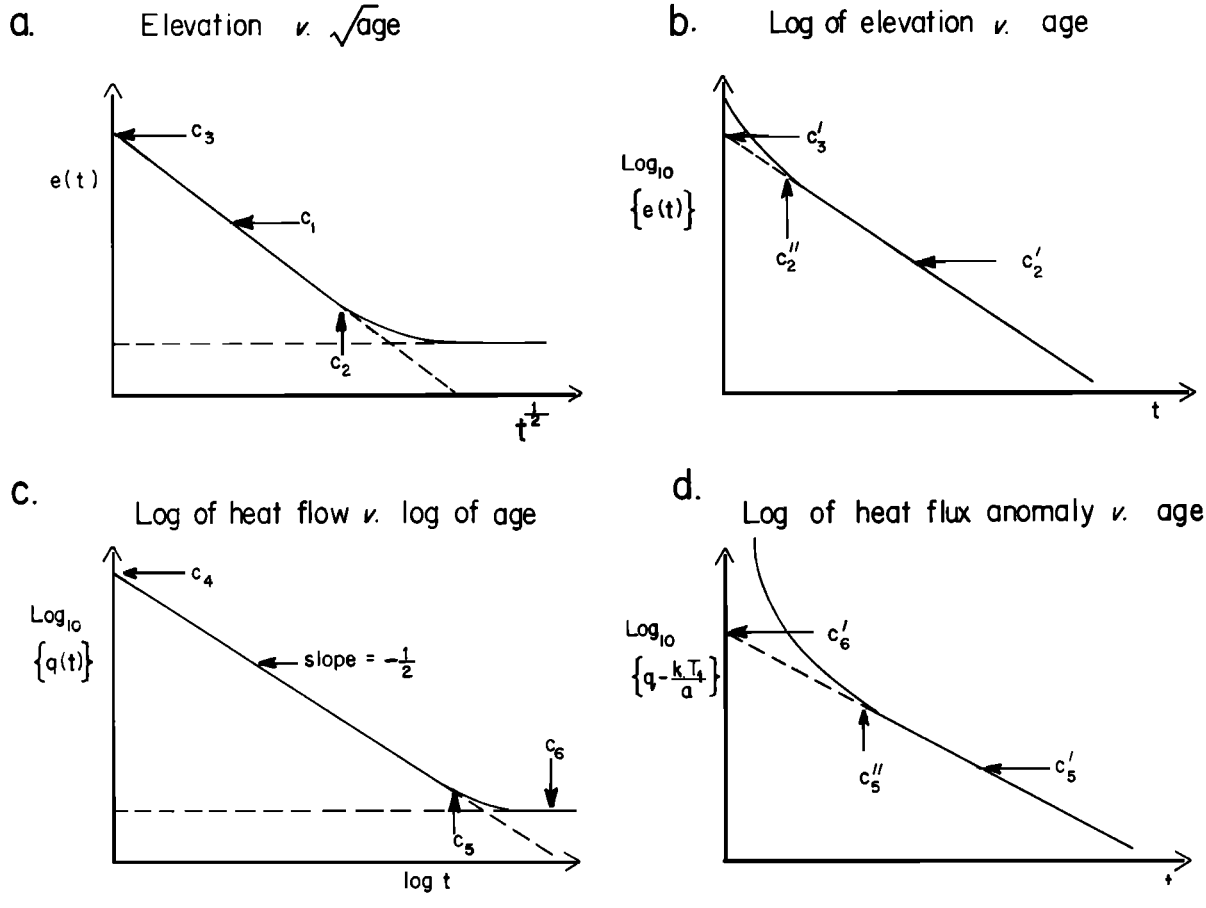

Fig. 5. A summary of the different ways that the data can be characterized in terms of the plate model. The various constants are discussed in the text and listed in Table 1.

In summary then, we can attempt to characterize the data as illustrated in Figure 5. It should be noted again that the characterization comes from the above analysis, which concerned itself with the behavior of a particular model, the plate model. The success with which the data can, in fact, be characterized in the fashion illustrated, and the agreement between independent estimates of the same numbers, provides a test of the model. By plotting the data in these different ways we can try to evaluate the constants illustrated in Figure 5. The principal ones are listed and defined in Table 1. The only one of the constants associated with the heat flow that we attempt to estimate is c_6, the value of the constant heat flux background. On examining the constants listed in Table 1 it can be seen that they provide only three independent relationships between lithospheric parameters. For instance, c_3 can be derived by using c_1 and c_2, and c_4 is related to c_5 and c_6. Therefore it is not possible to obtain all the lithospheric parameters from the data. We shall assume that ρ_o, ρ_w, C_p, and k are reasonably well known, and then from the estimated constants it is possible to derive values for a, T_1, and α. This approach enables the parameters to be calculated directly without having to fit curves to the data by eye, as is usually done.

Analysis of Topographic and Heat Flow Data

Presentation of the data. In young ocean floor, various models give similar predictions regarding the variation of heat flow and depth with age. The variation of depth with age out to about 80 m.y. B.P. can be accounted for by the plate model [Sclater et al., 1971]. However, it can equally well be accounted for by the cooling of a semi-infinite half space, no bottom boundary being required by the data [Davis and Lister, 1974], or by a model in which the bottom boundary is a liquid-solid phase transition and is allowed to migrate [Oldenburg, 1975]. As can be seen from the analysis in section 2, in young enough ocean floor, any of the thermal models will give the correct $t^{\frac{1}{2}}$ dependence, and to discriminate between the various models, the data set must be extended to greater ages. The main emphasis in this section is on the variation of depth with age, as we believe these data to be very reliable. Heat flow data for the same age range are also considered. Because the causes of scatter and low values in heat flow data are imperfectly understood, the methods used to extract reliable data points are still being developed. Hence we use the heat flow data only to demonstrate broad consistency with the model describing the topography.

TABLE 1. Estimate of Constants Characterizing the Data

Constant	Definition	Estimate			Equation		Figure
		Pacific	Atlantic				
C_1	$\frac{2\rho_o \alpha T_1}{(\rho_o - \rho_w)}\left(\frac{\kappa}{\pi}\right)^{\frac{1}{2}}$	354 ± 30	342 ± 65	$(\text{m.y.})^{\frac{1}{2}}$	(11)	Slope of depth versus $(\text{age})^{\frac{1}{2}}$	5a
C_2	$a^2/9\kappa$	64-80	64-80	m.y.	(14)	Breakdown of linear $t^{\frac{1}{2}}$ relation	5a
C_3	$\frac{\rho_o a \alpha T_1}{2(\rho_o - \rho_w)}$	3900 ± 200	3900 ± 350	meters	(11)	Intercept of elevation versus $(\text{age})^{\frac{1}{2}}$ for t = 0	5a
C_2'	$\frac{\pi^2 \kappa \log_{10} e}{a^2}$	0.0075 ± 0.0008	0.0066 ± 0.0015	1/(m.y.)	(16)	Slope of log (elevation) versus age	5b
C_3'	$\frac{4 a \rho_o T_1}{(\rho_o - \rho_w)\pi^2}$	3200	3200	meters	(16)	Intercept from log (elevation) versus age for t = 0	5b
C_4	$\rho_o C_p T_1 (\kappa/\pi)^{\frac{1}{2}}$	.....	.....	.....	(10)	Intercept at unit time from log (heat flow) versus log (age)	5c
C_5	$0.22a^2/\kappa$	.....	.....	.....	...	Age at which linear relationship for log (heat flow) versus log (age) breaks down	5c
C_6	kT_1/a	0.8 ± 0.1	0.8 ± 0.1	$\mu\text{cal cm}^{-2}\ \text{s}^{-1}$	(8)	Asymptotic constant value of heat flow	5c

Fig. 6. Mesozoic magnetic lineations, ship tracks with seismic reflection profiles, bathymetric contours, and DSDP sites in the northwestern Pacific Ocean. The lineations are based on Hilde et al. [1976], and Larson and Hilde [1975]. The bathymetric contours are from Chase et al. [1970] and are in uncorrected fathoms. Open triangles denote DSDP sites, listed in Table 2; solid triangles indicate that basement was reached. Solid circles denote the location of depth measurements.

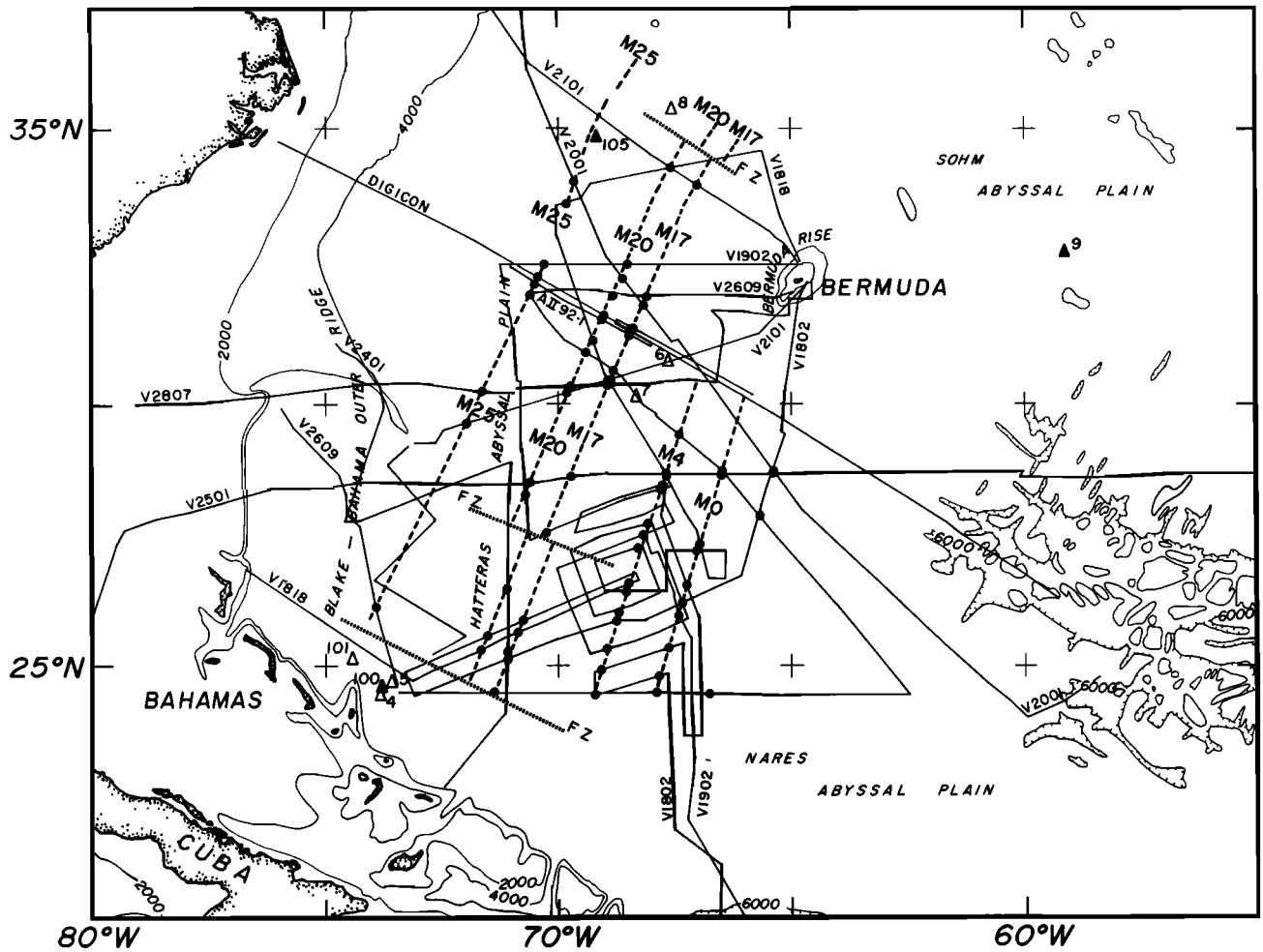

Fig. 7. Ship tracks with seismic reflection profiles in the western North Atlantic Ocean. The Mesozoic magnetic lineation pattern is discussed in the text. Bathymetric contours are in corrected meters and are taken from Uchupi [1971]. Other symbols are the same as those in Figure 6.

To extend the empirical depth-age curve, we have considered two areas where Mesozoic magnetic anomalies have been recognized. These are the North Pacific (Figure 6) and the western North Atlantic south of 34°N (Figure 7). In the North Pacific, mean depth values for ages less than 80 m.y. B.P. are tabulated in the work by Sclater et al. [1971]. Sclater and Detrick [1973] have given depths at a limited number of Deep-Sea Drilling Project (DSDP) sites. In Tables 2 and 3, depths at a more complete list of DSDP sites around the areas of interest are given. These tables serve two functions. One is to provide additional depth versus age values for comparison with those obtained from profiles. The second is to provide a check on our estimates of sediment thickness. The depths measured by using profiles are corrected for the loading effect of the sediments. This correction is particularly important in the older parts of the North Atlantic, where the sediment thickness exceeds 1 km. In Tables 2 and 3 the sediment thickness has been estimated where possible from seismic reflection profiles taken in the vicinity of the drill sites. In both areas there are a number of drill holes where basement was reached. The penetration in these cases provides a further check on the estimates of sediment thickness. Previously published isopach maps [Ewing et al. 1973; Lancelot and Larson, 1975] give sediment thicknesses in general agreement with our estimates. We used a sediment velocity (2 km s^{-1}) and density (1.7 g cm^{-3}) that will tend to give an upper limit to the correction for sediment loading, certainly for thicknesses less than 1 km. These steps were taken to prevent any bias toward too-shallow mean depths due to the sediment correction.

The Mesozoic lineations shown in Figure 6 are based on Hilde et al. [1976] and Larson and Hilde [1975]. Available ship tracks with seismic reflection profiles along them were superimposed over the map of the Mesozoic magnetic anomalies. Reflection profiles taken by the Glomar Challenger and on drill site surveys have been published in the Initial Reports of the Deep Sea Drilling Project (see Table 2 for sources). Other data points were obtained from unpublished Vema and Conrad (Lamont-Doherty Geological Observatory) profiles and from four parallel profiles across the Hawaiian lineations taken by the OSS Oceanographer during the NOAA western Pacific geotraverse project. We measured depths where these tracks crossed selected lineations provided that the lowermost reflector on the reflection profile could be identified as basement

with a reasonable amount of confidence, hence giving a reliable value for the sediment thickness. The depths were corrected to the true water velocity [Matthews, 1939] and then for the isostatic loading of the sediments. Mean values are presented in Table 4.

For the North Atlantic our treatment was slightly different. In these latitudes there are no mean depths available even for younger ocean floor, the data of Sclater et al. [1971] extending out only as far as 21 m.y. B.P. (anomaly 6). Therefore for ages out to 90 m.y. B.P. we have used mean values calculated from all the profiles between 34°N and 20°N, on both sides of the mid-Atlantic Ridge, presented by Sclater et al. [1975]. The 1° square averages of the free air gravity anomaly for these latitude limits are comparatively small. This choice, and averaging over many profiles, is made in an attempt to minimize any bias away from the true depth-age values. The second difference in treatment was in the location of the Mesozoic magnetic anomalies. In the North Pacific most of the Mesozoic anomaly sequence is quite clear, but this is not the case in the North Atlantic. Hence here we have measured depths at different anomalies from those used in the North Pacific. The onset of the quiet zone and the two groups of anomalies, M20-16 and M4-0, are generally more distinctive than the remainder of the sequence. Other parts of the Mesozoic anomaly sequence appear confused or even missing. We obtained plots of magnetic anomalies at right angles to ship track for tracks with seismic reflection profiles shown in Figure 7. Using identifications along the tracks for the anomalies given in Table 5, we measured depths and sediment thickness at the locations marked in Figure 7. The data sources are for the large part published Vema profiles [Talwani, 1974]. These have been supplemented by unpublished profiles (Digicon and AII-92-1) taken during surveys for the International Phase of Ocean Drilling (IPOD) project. We have also sketched in the trends of the Mesozoic lineations in Figure 7, based on our own identifications and the previous results of Vogt et al. [1971] and Larson and Hilde [1975]. Mean depths and sediment thicknesses for all ages in the North Atlantic are given in Table 5.

The mean depths are plotted against the square root of age in Figures 8a and 8b. Both areas show the same general features, initially an increase in depth varying linearly as $t^{\frac{1}{2}}$ and then in older regions a less rapid increase in depth appearing as a flattening of the curves. By using the mean depth points and taking into account the standard deviations, a best estimate of between 64 and 80 m.y. B.P. was obtained for the point of departure from the linear $t^{\frac{1}{2}}$ relationship. This behavior is close to that predicted by the plate model. Theoretical depths calculated by using the lithospheric parameters estimated later in this section are shown in Figures 8a and 8b; the agreement is quite reasonable. An approximate estimate for the age around which the linear relationship breaks down ($\sim$70 m.y. B.P.) gives 630 m.y. as the value for the parameter a^2/κ. From the asymptotic relation (16) an estimate of the final depth which would be reached in old enough sea floor can be made by using a few of the oldest points. With this depth as a base line the logarithm of elevation can be plotted versus age. This is done in Figures 9a and 9b, where a reference depth of 6,400 m has been used in both cases. A reasonable linear relation can be seen for ages larger than 20 m.y. B.P. The apparent increase in scatter for the older points is an effect of the logarithmic scale used. All the points lie within about 100 m of the linear relation for the North Pacific and within about 170 m for the North Atlantic.

Two final observations concerning the mean depth in the older regions can be made. First of all, the theoretical depth given by the plate model shows that, between 140 and 200 m.y. B.P., only a further 200 m increase in depth is to be expected. This magnitude for the remaining depth change lies within the scatter in the data. Second, the linear $t^{\frac{1}{2}}$ relation, if it is continued out to 160 m.y. B.P., predicts a depth of 7000 m. Consideration of the depth contours for the North Pacific (Figure 6) shows that for the most part the depth does not fall below 6000 m. Allowing for a reasonable mean sediment thickness of 400 m results in corrected depths less than 6,300 m. Thus there is a substantial difference between the observed behavior and that predicted by a linear $t^{\frac{1}{2}}$ relation, confirming the result displayed in Figures 8a and 8b.

If the topography can be accounted for by this simple cooling process, then one would expect the same model to describe the observed heat flow. However, there are many uncertainties associated with heat flow measurements. Values in poorly sedimented regions near ridge crests show a large scatter as a function of position, and the magnitudes of the measured values are considerably smaller than those predicted by the plate model [Talwani et al., 1971; Lister, 1972]. Very large values of heat flux (>30 μcal cm^{-2} s^{-1}) have been observed near the ridge crest in some places [Williams et al., 1974], and this suggests that most measurements in these regions are underestimates of the actual value. At present an explanation of both the scatter and the low values is being sought in terms of heat transport by water circulating in cracked rocks within a few kilometers of the ocean floor, either as convection within a porous medium or by heat exchange between individual cracks and ocean water [Lister, 1974]. The low values near ridge crests can be explained by assuming that a large proportion of the heat transport is due to water circulation, whereas the observations only give the conductive gradient in the sediments where the measurements are made.

With these cautionary remarks in mind we will make a comparison of available heat flow data and the predictions of the plate model. Values for the mean heat flow in given age zones, compiled with little selectivity with regard to the environment of the measurement, have been given by Sclater and Francheteau [1970] for the Pacific and South Atlantic and by McKenzie and Sclater [1971] for the Indian Ocean. These are plotted in Figure 10. Also shown are estimates of the heat flow in the North Pacific that were obtained after considering the environment of all the individual measurements [Sclater et al., 1976] and they are considered more reliable. Recent studies [Lister, 1972; E.E. Davis and C.R.B.

TABLE 2. Depth and Sediment Thickness at Joides Drill Holes in the Northwestern Pacific with Magnetic Anomaly or Biostratigraphic Ages

Site	Latitude	Longitude	Depth, m	Sediment Thickness Estimated From Profiles*, m	Penetration, m	Sediment Correction*, m	Corrected Depth, m	Biostratigraphic Zone or Comments	Magnetic Anomaly†	Age†, m.y.B.P.	Comments on Seismic Record
45	24°15.9'N	178°30.5'W	5508	600	105	420	5928	...	M3-4	115	Not clear
46	27°53.8'N	171°26.3'E	5769	400	9	280	6049	Close to Fracture Zone	M15	133	Clear
51	33°28.5'N	153°24.3'E	5981	400	132	280	6261	Edge of Shatsky Rise, Topographic Relief Large	M17	137	Clear
52	27°46.3'N	147°07.8'E	5744	(300)	69	210	5954	...	M24-25	152	Basement estimate given in site report
61‡	12°05.0'N	147°03.7'E	5570	135	98#	95	5665	On Trench Outer Rise	...	...	Clear, probably 30 m more sediment to basement
66‡	2°23.6'N	166°7.3'W	5293	235	192#	134	5427	Turonian or Cenomanian, Pronounced Basement High	...	87-100	Clear
164	13°12.1'N	161°31.0W	5499	300	264#	185	5684	Barremian-Albian	...	100-118	Clear
165	8°10.7'N	164°51.6W	5053	500	470#	329	5382	>Campanian, Edge of Line Islands	...	75-85	Clear
166‡	3°45.7'N	175°04.8'W	4962	350	307#	215	5177	On 300 - 500 m High Rise	M8	120	Clear
169	10°40.2'N	173°33.0'E	5407	300	233#	163	5570	Late Albian	...	100-104	Clear
170	11°48.0'N	177°37.0'E	5792	200	192#	134	5926	Late Albian	...	100-104	Clear
194	33°58.7'N	148°48.6'E	5744	400	256	280	6024	...	M17	137	Clear
195	32°46.4'N	146°58.7'E	5958	450	392	315	6273	...	M18-19	140	Clear
196	30°07.0'N	148°34.5'E	6184	400-750	377	525	6709	...	M22	148	Faint Reflector at 750 m on Aries 7 profile
197	30°17.4'N	147°40.5'E	6143	300	278#	195	6338	...	M23	150	Poor
199‡	13°30.8'N	156°10.3'E	6090	>300	465	350(est)	6440	In Trough Next to Large Guyot	...	...	Unclear
303	40°48.5'N	154°27.1'E	5609	300	285#	200	5809	Hauterivian	M4	117	Very clear
304	39°20.3'N	155°04.2'E	5630	300	335#	235	5865	Hauterivian	M9	121	Very clear
307	28°35.3'N	161°00.3'E	5696	350	297#	208	5904	Tithanian-Berriasian	M21	145	Clear

Data are from Fischer et al. [1971], Winterer et al. [1971, 1973], Heezen et al. [1973], and Larson et al. [1975].

*Assuming sediment velocity of 2 km/s and density of 1.7 g cm^{-3}. For these sediment thicknesses this generally overestimates the thickness and provides an upper limit on the loading effect.

†Based on lineations of Larson and Chase [1972] and Hilde et al. [1976], with time scale from Larson and Hilde [1975].

‡These sites have not been plotted in Figure 13.

#At these sites, basalt was drilled, and unless otherwise stated, the evidence was that this was basement. Penetration in these cases is to the top of the basalt.

TABLE 3. Depth and Sediment Thickness at Joides Drill Holes in the North Atlantic With Magnetic Anomaly or Biostratigraphic Ages

Site	Latitude	Longitude	Depth, m	Sediment Thickness Estimated From Profiles*, m	Penetration, m	Sediment Correction*, m	Corrected Depth, m	Biostratigraphic Zone or Comments	Magnetic Anomaly†	Age†, m.y.B.P.	Comments on Seismic Record
4	24°28.7'N	73°47.5'W	5320	500	259	350	5670	...	M25	153	Reasonably clear
5	24°43.6'N	73°38.5'W	5361	500	279	350	5711	...	M25	153	Reasonably clear
6‡	30°50.4'N	67°38.9'W	5125	1000	257	700	5825	...	M12	128	Not clear
7‡	30°08.0'N	68°17.8'W	5185	700	296	490	5675	...	M15	133	Clear
8‡	35°23.0'N	67°33.2'W	5169	700	314	490	5659	...	M25	150	Line drawing
9‡	32°46.4'N	59°11.7'W	4965	950	835#	585	5550	Maastrichtian	...	104	Line drawing
10‡	32°51.7'N	52°12.9'W	4697	500	457#	320	5017	Lower Campanian	...	77	Line drawing
11‡	29°56.6'N	44°44.8'W	3556	300	282#	197	3753	Middle Miocene	...	19	Line drawing
100	24°41.3'N	73°48.0'W	5325	320	317#	222	5547	Callovian-Oxfordian	>M25	155	Clear
101‡	25°11.9'N	74°26.3'W	4868	1060	691	742	5610	...	Jurrassic quiet zone	∿160	Clear
105	34°53.7'N	69°10.4'W	5251	650	623#	436	5687	Oxfordian	M25	153	Reasonably clear
112	54°01.0'N	46°36.2'W	3657	800	662#	463	4120	Late Paleocene early Eocene	26	65	Clear
114	59°56.0'N	26°48.0'W	1927	850	623#	436	2363	Late Miocene-early Pliocene	close to 5	12	Clear
115‡	58°54.4'N	21°07.0'W	2883	1000	228	700	3583	...	22	56	Line drawing
118‡	45°02.7'N	9°00.6'W	4901	>700	757#	530	5431	Late Paleocene	...	...	Basement not apparent
136‡	34°10.1'N	16°18.2'W	4169	370	308#	216	4385	Madeira Islands platform, oldest sediment early Aptian	...	140	Clear
137	25°55.5'N	27°03.6'W	5361	400	397#	278	5639	Late Albian	...	111	Clear
138	25°55.4'N	25°33.8'W	5288	500	437#	350	5638	Cenomanian	...	120	Clear, probably a sill with 50 m more sediment below
332‡	36°52.8'N	33°38.6'W	1806	150	142#	99	1905	...	2'-3	3.5	Line drawing
333‡	36°50.5'N	33°40.1'W	1666	250	219#	153	1819	...	2'-3	3.5	Line drawing
334‡	37°02.1'N	34°24.9'W	2632	300	259#	181	2813	...	5	8.9	Line drawing
335‡	37°17.7'N	35°11.9'W	3198	550	454#	318	3516	...	>5	16.5	Line drawing
367‡	12°29.2'N	20°02.8'W	4748	1200	1140#	798	5546	Oxfordian-Kimmeridgian	...	...	Line drawing

Data are from Ewing et al. [1969], Peterson et al. [1970], Hollister et al. [1972], Laughton et al. [1972], Hayes et al. [1972], and Scientific Staff [1974, 1975].

*Assuming sediment velocity of 2 km/s and density of 1.7 g cm^{-3}. The sediment velocity and density assumed are now more appropriate for the greater thickness of sediment encountered than they are in Table 2.

†Ages from Pitman and Talwani [1972] and Larson and Hilde [1975] using nearby magnetic anomalies or, in some instances, interpolation between isochrons.

‡These sites have not been plotted in Figure 13.

#At these sites, basalt was drilled, and unless otherwise stated, the evidence was that this was basement. Penetration in these cases is to the top of the basalt.

TABLE 4. Mean Depth Versus Age From Profiles in the North Pacific

Age*, m.y.	Anomaly*	Number of Values	Mean Depth, Corrected Meters	Mean Sediment Thickness, m	Mean Depth Corrected for Sediment Loading, m	Standard Deviation, m
117	M4	3	5427	450	5742	143
126	M11	8	5784	394	6061	153
133	M15	7	5887	400	6167	105
143	M20	8	5785	381	6051	99
153	M25	4	5875	381	6147	109
163	JQZ+	3	5926	317	6148	168

*Identification of anomalies and ages based on Larson and Hilde [1975] and Hilde et al. [1976].

+JQZ, Jurassic quiet zone.

Lister, unpublished manuscript, 1976; Sclater et al., 1976] have shown that in areas with uniform reasonably thick sediment cover (>200 m), heat flow measurements were much less scattered than those measured in areas with outcropping basement highs and thin patchy sediment cover. Also the mean of these measurements alone tends to be significantly larger than that obtained by using all heat flow values regardless of environment. A similar effect is observed in the reduction of the standard deviation associated with the mean heat flow as the age increases, the sediment cover generally increasing in thickness with age. These observations suggest that a sufficiently thick sediment cap effectively seals off cracks in the underlying basement and strongly influences any remaining effects of hydrothermal circulation. The reliable means plotted in Figure 10 were obtained by using only heat flow measurements taken in areas with a uniform sediment cover greater than 200 m thick [Sclater et al., 1976].

Figure 10 demonstrates that the earlier values obtained without regard to the environment were very scattered. These values are also significantly lower than the heat flow predicted by a plate model that satisfies the topographic data using parameters discussed later in this section. The more reliable means, however, show good agreement with the predicted values. These latter means only, and the theoretical curve, have been replotted in Figure 11 as the logarithm of heat flow versus the logarithm of age. A straight line with a slope of $-\frac{1}{2}$ provides a good fit over the age range of most of the data. The age at which the predictions of the plate model begin to differ from the $t^{-\frac{1}{2}}$ relation is around 120 m.y., about twice the age at which the linear $t^{\frac{1}{2}}$ variation of the depth breaks down as discussed in section 2. It can be seen from Figure 11 that the difference between the prediction of the plate model and the continuation of the $t^{-\frac{1}{2}}$ dependence for ages larger than 120 m.y. are very small. The difference is less than 0.1 μcal cm^{-2} s^{-1} until about 165 m.y., and hence discrimination between the two on the basis of heat flow will be difficult. We therefore have the surprising conclusion that although the plate model was originally suggested by the apparently constant heat flow for old ocean floor, its justification comes not from the heat flow data at all but from the bathymetric data.

Estimation of lithospheric parameters. Some of the constants defined in section 2 can now be obtained from the plots in Figures 8-11. These are given in Table 1. The errors also given are estimated from the graphs. They should not be regarded as true statistical errors, although in the calculations they are treated as such, but as a subjective measure of the uncertainty in the values. Relationships between different constants provide a check on the consistency with which the plate model describes the data. For instance, Table 6 lists the results of three different methods of estimating the parameter a^2/κ for both the Pacific and the Atlantic data. These make use of the age of the breakdown of the linear $t^{\frac{1}{2}}$ relation, the slope of the asymptote in the plot of the logarithm of elevation versus age, and, third, the ratio of the ridge crest elevation to the slope of the linear $t^{\frac{1}{2}}$ relation. The different values are in reasonable agreement, although the third method is more sensitive to errors in the constant values used. In subsequent calculations a value of 620±100 m.y. will be used for the Pacific, and 650±100 m.y. for the Atlantic. An age equal to one tenth of this value gives a measure of the thermal time constant of the lithosphere. Another, less important, check comes from the ratio c_3'/c_3, the actual value of 0.82 lying close to the theoretical value of $8/\pi^2$ given by (11) and (16).

The value of c_6, the asymptotic heat flow

TABLE 5. Mean Depth Versus Age From Profiles in the North Atlantic South of 34°N

Age*, m.y.	Anomaly*	Number of Values	Mean Depth, Corrected Meters	Mean Sediment Thickness, m	Mean Depth Corrected for Sediment Loading, m	Standard Deviation, m
0	1	12	2528	-	2528	247
		(9)	(2599)		(2599)	(235)
10	5	24	3395	40	3423	315
		(18)	(3542)	(6)	(3546)	(251)
38	13	24	4500	95	4567	378
		(18)	(4702)	(49)	(4736)	(217)
53	21	24	4889	121	4974	421
		(18)	(5106)	(83)	(5164)	(210)
63	25	24	5118	143	5218	447
		(18)	(5327)	(97)	(5395)	(264)
72	31	24	5298	199	5437	437
		(18)	(5493)	(151)	(5599)	(308)
82	33	24	5331	225	5489	424
		(18)	(5453)	(195)	(5590)	(411)
90	CQZ+	23	5409	280	5605	403
		(17)	(5459)	(259)	(5640)	(456)
101	CQZ+	4	5442	388	5713	214
109	M0	10	5427	410	5714	222
117	M4	15	5340	587	5751	243
137	M17	17	5333	806	5897	224
143	M20	15	5371	817	5943	212
153	M25	9	5389	1172	6209	271

Numbers in parentheses were obtained by excluding profiles north of 31°N from the the data set of Sclater et al. [1975].
*Time scale from Heirtzler et al. [1968] and Larson and Hilde [1975].
+CQZ, Cretaceous quiet zone.

background, was estimated as follows. A contribution of 0.1 HFU (μcal cm^{-2} s^{-1}), considered as the contribution due to radioactive heating in the lithosphere, was subtracted from the oldest of the heat flow means. Strictly speaking, if we are to account for lithospheric radioactive heating, we should use an alternative expression to (8) allowing for the effect of the internal heating on the geotherm. However, the error made in neglecting to do this is small compared with the final error in the estimated value of T_1 due to errors in the values of the constants, so the simple form for c_6 is retained. Using the estimates of the time constant $a^2/\pi^2\kappa$, the background heat flux was then calculated by using the asymptotic relation (17). This shows that the cooling of the lithosphere down to equilibrium still contributes 0.2 HFU of the observed heat flux, leaving 0.8 HFU for the background value. This is smaller than pervious estimates [Sclater and Francheteau, 1970], which did not correct for any further decay before reaching equilibrium.

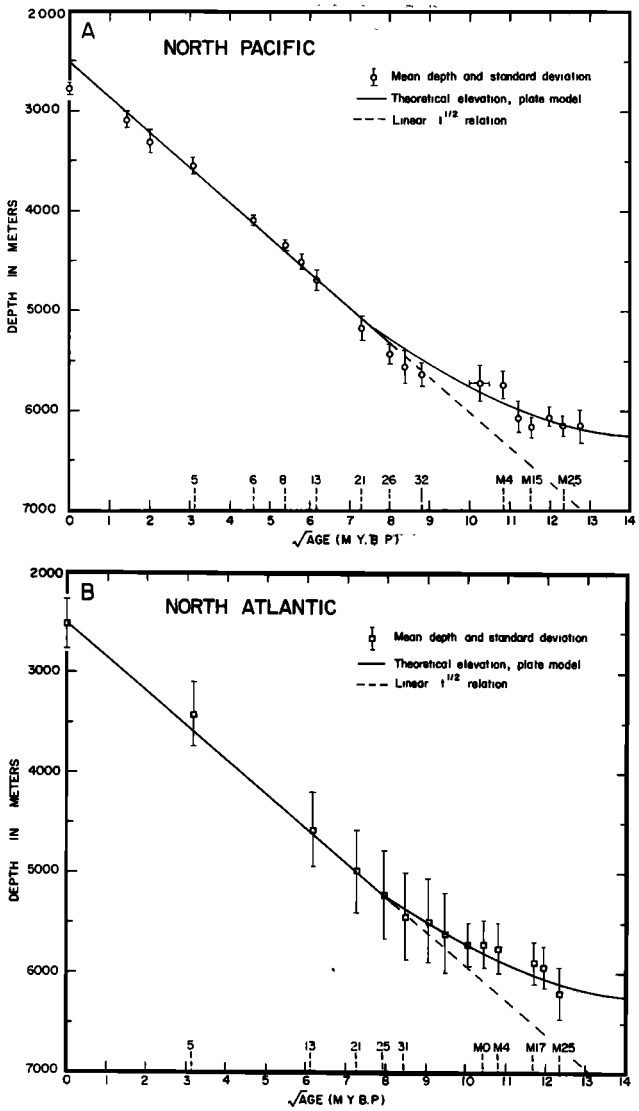

Fig. 8. Mean depths and standard deviations plotted versus the square root of age for (a) the North Pacific and (b) the North Atlantic. Predicted values for a linear $t^{\frac{1}{2}}$ dependence and for a plate model using lithospheric parameters discussed in the text are given. An additional point in the Cretaceous quiet zone was obtained by averaging depths at DSDP sites 164, 169, and 170; this is denoted by the error bar on age.

Values for the following physical quantities are needed in order to estimate the lithospheric parameters:

$$\rho_o = 3.33 \text{ g cm}^{-3}$$
$$\rho_w = 1.0 \text{ g cm}^{-3}$$
$$C_p = 0.28 \text{ cal g}^{-1} \text{ °C}^{-1} \qquad (18)$$
$$k = 7.5 \times 10^{-3} \text{ cal °C}^{-1} \text{ cm}^{-1} \text{ s}^{-1}$$

The specific heat is based on measurements of typical minerals over temperatures appropriate for the upper part of the lithosphere [Goranson, 1942] and an upper limit of 0.295 cal g^{-1} $°C^{-1}$ given by Dulong and Petit's law for olivine. The value for the thermal conductivity is a mean value for the upper 120 km of the mantle estimated from the results of Schatz and Simmons [1972]. Using these values, we can calculate successively the lithospheric thickness a from the estimate of a^2/κ, then T_1, using the definition of c_6, and last, the thermal expansion coefficient α from the definition for c_3. The resulting best fitting parameters for the North Pacific are

$$a = 125 \pm 10 \text{ km}$$
$$T_1 = 1333° \pm 274°C \qquad (19)$$
$$\alpha = (3.28 \pm 1.19) \times 10^{-5} \text{ °C}^{-1}$$

and for the North Atlantic,

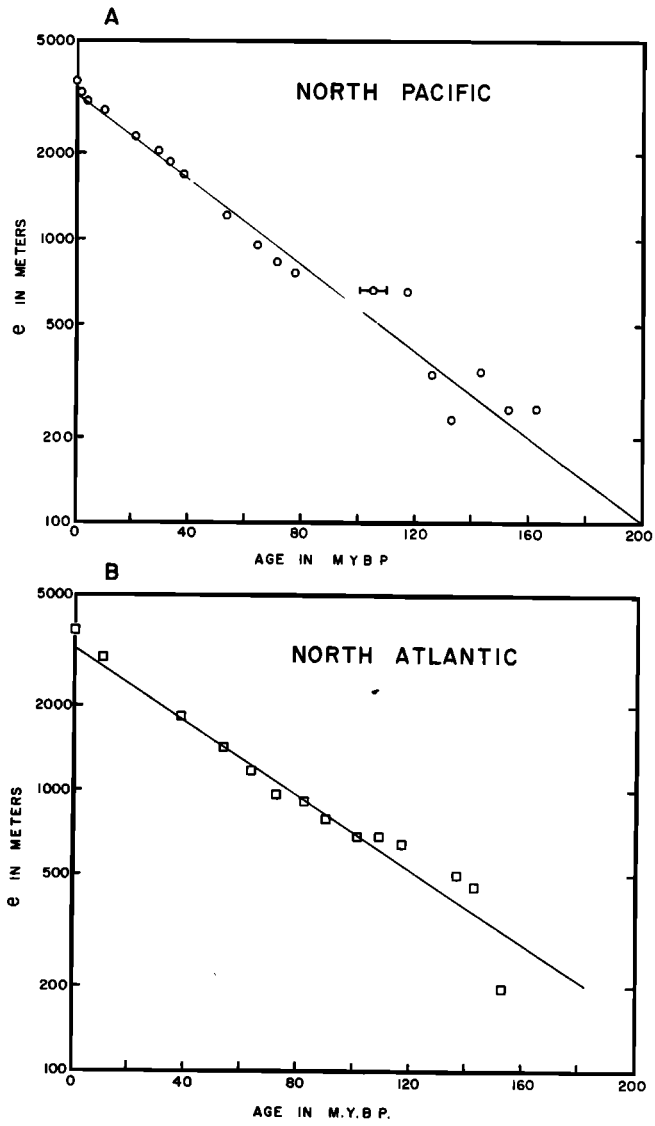

Fig. 9. Mean elevations plotted on a logarithmic scale versus age for (a) the North Pacific and (b) the North Atlantic. In both cases a reference depth of 6400 m has been used to give the elevation.

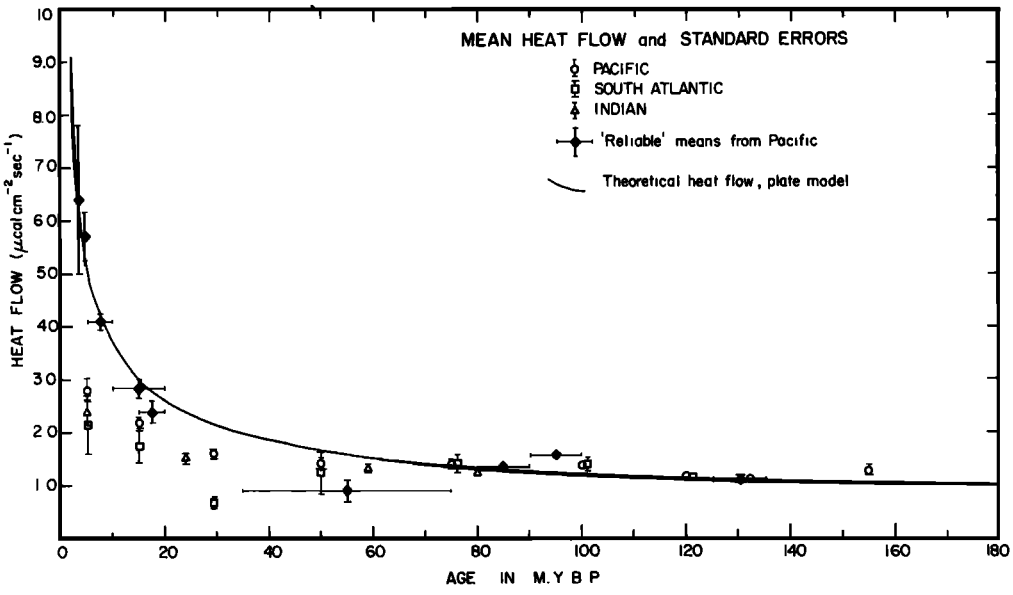

Fig. 10. Standard heat flow averages plus the more selective means of Sclater et al. [1976] plotted as a function of age. The theoretical curve is calculated using the parameters (19) estimated in the text.

$$a = 128 \pm 10 \text{ km}$$

$$T_1 = 1365° \pm 276°C \qquad (20)$$

$$\alpha = (3.1 \pm 1.11) \times 10^{-5} \text{ °C}^{-1}$$

The values given by (19) and (20) are those that have been used in calculating the theoretical curves in Figures 8-11. It should be noted that the relative uncertainty increases in going from a to T_1 and then α, as the errors in the parameters include the error in the parameter estimate that preceded it as well as the error in the values of the constants. The error estimates are derived from the same relationships that define the constants (Table 1). In estimating the different errors, no account has been taken of possible uncertainties in the assumed parameters given by (18). The thickness is the best constrained of the three parameters. The estimate of the thermal expansion coefficient agrees well with measured values for typical lithospheric minerals [Skinner, 1966]. However, throughout this paper we have ignored the possible contribution of phase changes to the elevation. In the calculations of both Sclater and Francheteau [1970] and Forsyth and Press [1971] the phase changes made a substantial contribution to the elevation, yet the above calculations show that the topographic data can be perfectly well explained without taking this into account. Furthermore, we have seen that a linear relation with respect to $t^{\frac{1}{2}}$ holds well out to 70 m.y. B.P. Either the effect of the phase changes on the elevation is negligible or the nature of the phase boundaries present are such that the phase boundaries initially approach their final level as $t^{\frac{1}{2}}$, so that the linear $t^{\frac{1}{2}}$ relation in the depth is preserved [Davis and Lister, 1974].

It is commonly assumed in plate calculations that the bottom boundary of the lithosphere is associated with partial melting, which occurs throughout the low-velocity zone. Once the thickness of the lithosphere is specified, these calculations obtain the bottom boundary temperature from a given solidus. This procedure can be reversed here, as both the thickness and the temperature have been estimated independently. The weight of evidence favors an overall peridotitic composition for the upper mantle. In Figure 12 we have plotted various melting curves for peridotite taken from Kushiro et al. [1968]. The depth and temperature estimated for the base of the plate model fall closest to curve B, the solidus appropriate in the presence of water occurring as hydrous minerals rather than as free water. A more appropriate curve for the onset of partial melting may be C, appropriate when free water is present as a phase in the upper mantle. This implies that the base of the plate as defined by the thermal models is deeper than the depth at which partial melting occurs.

Finally, the simple square root and exponential asymptotes for young and old ocean floor provide the basis for simple empirical formulae. For young ocean floor the depth is given by

$$d(t) = 2500 + 350(t)^{1/2} \text{ m} \qquad (21)$$

with t in m.y. B.P., this relationship holding for $0 < t < 70$. For older ocean floor the depth is described by

$$d(t) = 6400 - 3200 \exp(-t/62.8) \text{ m} \qquad (22)$$

which is a good approximation for $t > 20$ m.y. B.P. In the case of the heat flow, only the $t^{-\frac{1}{2}}$ dependence illustrated in Figure 11 has been tested at all adequately. This gives a relationship

$$q(t) = 11.3/t^{1/2} \text{ μcal cm}^{-2} \text{ s}^{-1} \qquad (23)$$

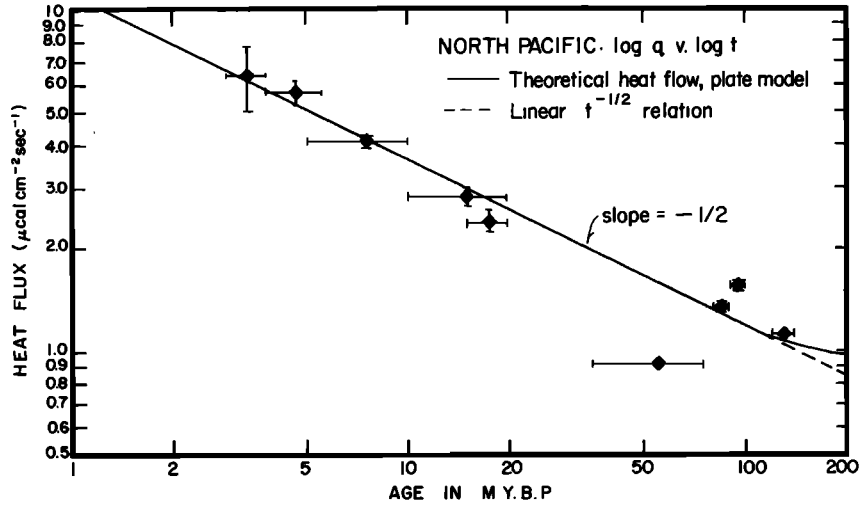

Fig. 11. The reliable heat flow means, calculated using measurements in uniformly well-sedimented areas, plotted on a logarithmic scale versus age and also on a logarithmic scale. The theoretical curve has a slope of -1/2 until an age of about 120 m.y. B.P. The small differences between the plate model values and the continuation of the $t^{-\frac{1}{2}}$ dependence can be seen.

valid for $0 < t < 120$ m.y. B.P. This is in agreement with the result given by Lister [1975].

Discussion

It has been demonstrated that, for sufficiently large ages, the depth increases less rapidly than predicted by a linear $t^{\frac{1}{2}}$ dependence. We would like to infer from this flattening of the depth-age curve that it is necessary to supply heat from the mantle to the base of the plate. Before doing so, however, it is necessary to discuss possible difficulties that could make this inference uncertain and to provide reasons why these difficulties are unlikely to affect the basic conclusions. In the critical region, for ages larger than 80 m.y. B.P., the values of mean depths are very reliable, but the flattening seen in Figures 8a and 8b also depends on the time scale [Larson and Hilde, 1975] used to assign ages to the Mesozoic lineations. The Jurassic time scale is still under development [van Hinte, 1976], and some uncertainty exists in the ages. Berggren et al [1975], in their discussion of the original time scale for the Mesozoic lineations put forward by Larson and Pitman [1972, 1975], proposed differences in the ages assigned to the Mesozoic anomalies based on van Hinte's [1976] time scale and control points provided by basement contacts at DSDP sites. In this way, they removed the necessity for worldwide changes in the spreading rate required using the time scale of Larson and Pitman [1972]. Regardless of whether one agrees with the views of Berggren et al. [1975] or those of Larson and Pitman [1975], the maximum difference between the time scales (13 m.y.) provides a good upper bound on any errors. The interval of time represented by the late Jurassic stages (7 m.y.) is assigned somewhat arbitrarily [Larson and Hilde, 1975]. However, considering the control provided by combining radiometric dates, biostratigraphy, and magnetic stratigraphy [van Hinte, 1976], the errors are unlikely to be larger than the 7 m.y. span of these stages. Furthermore, these errors refer to internal inconsistencies within the Mesozoic time scale and not to bodily shifts to earlier times. The radiometric dating providing control generally gives minimum ages. To bring the older points in Figures 8a and 8b onto the $t^{\frac{1}{2}}$ line requires shifts of between 25 and 50 m.y. to earlier ages, and this would appear to be highly unlikely.

TABLE 6. Results of Different Methods of Estimating a^2/κ

Method	a^2/κ, m.y. Pacific	a^2/κ, m.y. Atlantic	Equation
$9c_2$	648 ± 72	648 ± 72	(14)
$\frac{\pi^2 \log_{10} e}{c_2'}$	570 ± 60	647 ± 147	(16)
$\frac{16}{\pi}\left[\frac{c_3}{c_1}\right]^2$	620 ± 200	660 ± 330	(11)

Thus the flattening in Figures 8a and 8b is real, but can this immediately be used to infer a similar flattening in the thermal structure of the lithosphere? Another alternative is that a systematic thickening of the crust with age causes the observed variation of depth with age, while the thermal structure is unchanged from that which would produce the $t^{\frac{1}{2}}$ dependence in the depth. We believe there are three reasonable arguments that this is not the case. Primarily, there is no convincing observational evidence that the crust systematically thickens [Christensen and Salisbury, 1975; Woollard, 1975; Tréhu et al., 1976]. Undoubtedly, there is considerable variation of crustal thickness from place to place, but no general increase in total

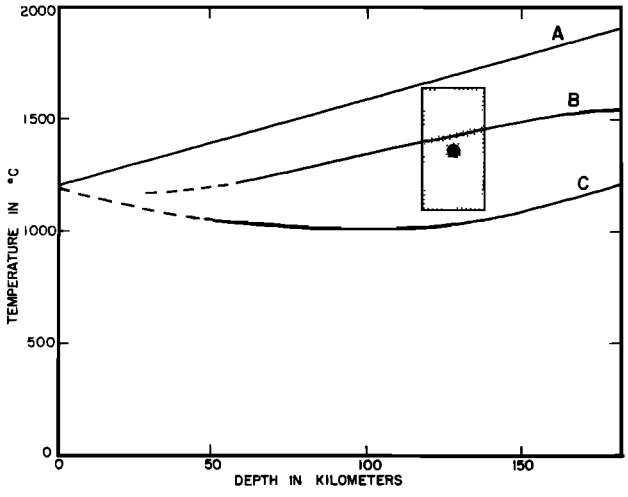

Fig. 12. Best estimate (solid circle) and range of errors (shaded area) for the temperature and depth of the bottom boundary of the plate compared with melting point curves from Kushiro et al. [1968]. Curve A is the solidus for anhydrous conditions, B is that for hydrous conditions with $P_{H_2O} \ll P_{load}$, and C is the melting curve corresponding to the case where free water is present as a phase.

thickness with age. Tréhu et al. [1976] have shown that increases in thickness of the order required to produce the observed variation in the depth with age are clearly ruled out by the observations in the North Atlantic. Second, in the absence of any convincing observational evidence for increases in crustal thickness one ought to put forward a mechanism by which the crust could be systematically thickened. A currently accepted model for crustal production is that of extensive partial melting of a peridotitic mantle and the bleeding off of the melt [Wyllie, 1971]. Such a model could easily account for the variations in crustal thickness due to fluctuations in the intrusion process at the ridge crest. Evidence from seismic attenuation [Solomon, 1973] suggests that the zone of extensive partial melting is confined to the immediate vicinity of the ridge crest, and there is no evidence for larger than a small amount of partial melting elsewhere. Hence it is hard to see how the crust could be systematically thickened within the context of this mechanism. Finally, even if we could derive a mechanism, it would have to be such as would only produce significant effects for ages older than 70 m.y. B.P. and not where the linear $t^{\frac{1}{2}}$ dependence still holds.

The last point that we wish to make with regard to the data concerns ways in which estimates of the mean depths at given ages can be improved. It is evident that ocean floor of a given age is not all at exactly the same depth, but there is a certain amount of scatter about the mean value. This is illustrated in Figures 13a and 13b, where the individual measurements used in calculating the mean depths are plotted as well as depths at DSDP drill sites from Tables 2 and 3 and Sclater and Detrick [1973]. The variations of depth around the mean value could have various causes, among them the effects of mantle convection beneath the plate [Sclater et al., 1975; Watts, 1976] and the results of variation in crustal thickness produced in the intrusion process at the ridge crest [McKenzie and Bowin, 1976]. In including data points for averaging one usually excludes areas with structures that are far from being normal oceanic crust, e.g., the Shatsky rise, for want of sufficient knowledge that would enable the depth to be corrected, as one does in the case of sediment loading. However, it is clear that areas with otherwise normal oceanic structures but which appear much too shallow or too deep should not necessarily be excluded. Until one knows the exact mean value at a given age a judgement cannot be made as to whether a given point is deeper or shallower than average. Also to omit such points may result in the mean depths becoming biased. It seems preferable to include depth measurements with as large a coverage as possible and to obtain an independent check on any possible bias. This could be provided by calculating an average free air gravity anomaly associated with the mean depth, using gravity values at all the points at which the depth is measured. An unbiased mean depth should be associated with a mean free air gravity anomaly close to zero. Differences from zero would enable an estimate of the bias in the depth to be made by using the slopes of observed relations between gravity and topography [Sclater et al., 1975; McKenzie and Bowin, 1976]. In the North Pacific, measurements with a sufficiently wide coverage from areas with generally small gravity anomalies have been used and should provide a good estimate of the mean depth. Our concern with the above points stems from the difficulties in isolating depth-age information in the North Atlantic. Here there are commonly accepted to be large disturbances in the depth, possibly due to crustal variations and mantle convection. In Table 5 we also give mean values for ages less than 90 m.y. B.P. when profiles north of 31°N are excluded. The basic shape of the curve is unchanged, but mean values deepen by up to 200 m, and also the scatter is reduced (Figure 13b). A method such as that described above would indicate how much other processes have affected the depth-age values.

We conclude therefore that there is a real departure of the variation of depth with age from a linear $t^{\frac{1}{2}}$ dependence and that this requires an input of heat flux at the base of the lithosphere. The estimates made in section 3 for the time constant a^2/κ indicate that the thermal structure begins to feel the influence of some bottom boundary condition at a depth between 115 and 135 km. The simple $t^{\frac{1}{2}}$ dependence initially observed in the depth variation eventually breaks down. Its importance remains, however, for, together with the observation of topographic ramps in regions where jumps in the spreading center have occurred [Sclater et al., 1971; Anderson and Sclater, 1972; Anderson and Davis, 1973], it provides substantial proof of the thermal origin of the broad variations in ocean depth with age.

Both the variation of the mean depth with age and that of the reliable heat flow averages can be described by the same plate model. The

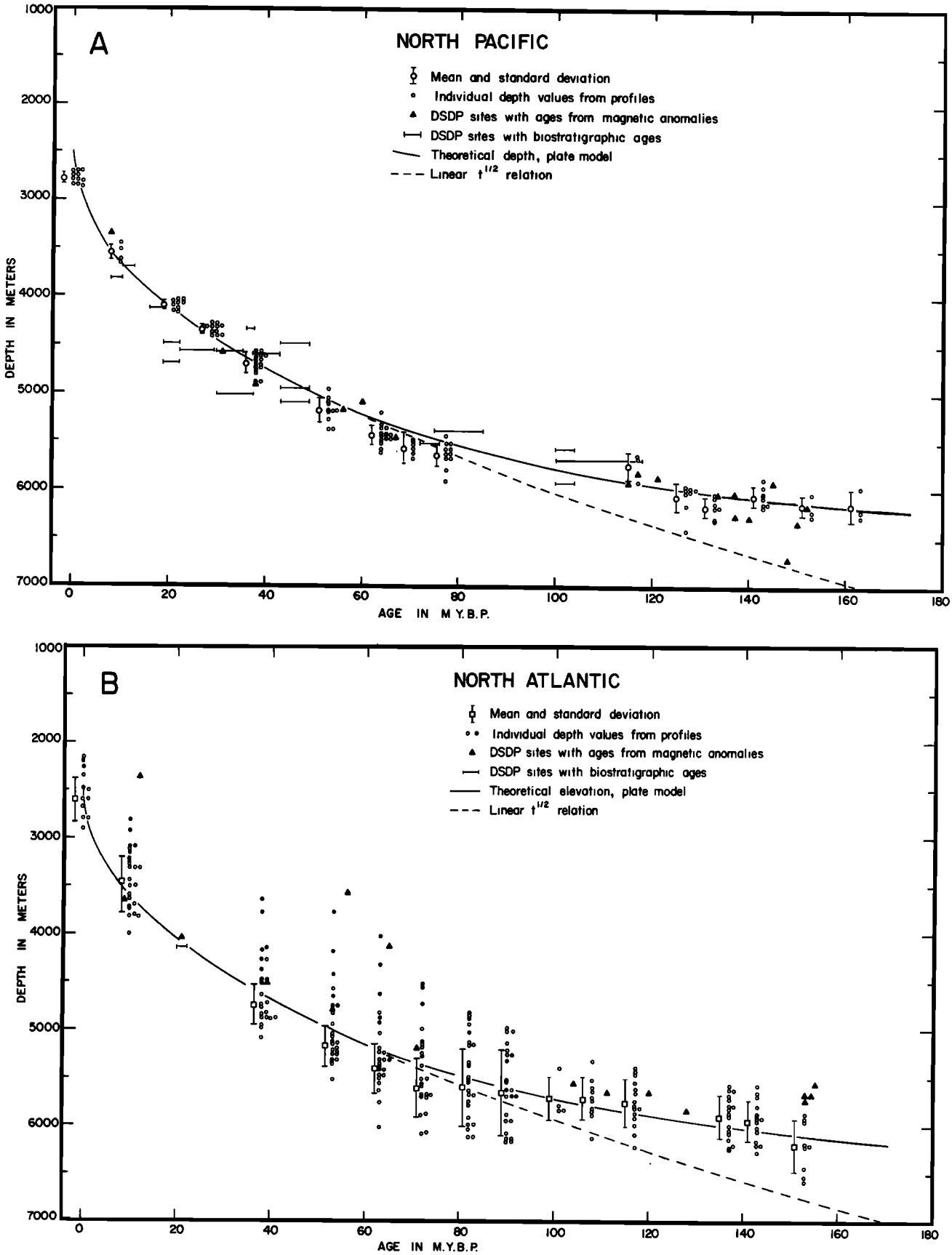

Fig. 13. Plot of individual depth measurements used in calculating mean depths and depths at DSDP sites for (a) the North Pacific and (b) the North Atlantic, illustrating the scatter in depths about the mean value. The means and standard deviations from the individual profile measurements are offset 2 m.y. The correct age is represented by the first column of individual points, some points being slightly offset for clarity. The solid circles in Figure 13b are points from profiles north of 31°N in the data set of Sclater et al. [1975].

essential component of the plate model is that at a depth of about 125 km the temperature remains essentially constant and the topography is compensated. The simple mathematical framework is found to provide a reasonable description of the data, although the question of the physical maintenance of such a picture is avoided. In order to keep the temperature constant at a given depth, heat must be supplied from below to compensate for that lost by cooling. The term 'plate model' implies nothing regarding the mechanism by which this heat is supplied. In the introduction we suggested one possible method, that of small-scale mantle convection [Richter, 1973; Richter and Parsons, 1975; McKenzie and Weiss, 1975]. The details of the development of the thermal structure of the lithosphere when small-scale convection transports heat in the upper mantle, and means of discriminating between this mechanism and other possible alternatives, are discussed elsewhere (B. Parsons and D. McKenzie, manuscript in preparation, 1976).

The results obtained here can be tested in the following ways. Further measurements of depth and sediment thickness, together with control provided by gravity measurements, in the areas studied, and in other areas where Mesozoic lineations have been identified, should be made to check the mean values given here. We have pointed out that the differences between the heat flow predicted by the plate model and a continuation of the $t^{-\frac{1}{2}}$ dependence in the older regions are very small and they may be very difficult to detect. However, the causes of scatter are certainly not fully understood, and the exact way that increasing thicknesses of sediment influence hydrothermal circulation has to be determined. Hence the systematic measurement of a large number of heat flow values with carefully studied environments in the old ocean basins may yet provide sufficiently accurate mean heat flow estimates. The third way of obtaining constraints on the thermal evolution of the lithosphere is from seismic evidence. Shear wave velocities are very sensitive to the onset of partial melting, and measurements of the shear wave velocity distribution in different age zones [Leeds et al., 1974; Forsyth, 1975] enable the depth to this boundary to be determined as a function of age. This depth does not necessarily coincide with the depth determined by fitting the topographic data, as was illustrated in section 3, and its variation with age is also affected by the exact shape of the melting curve as a function of temperature and pressure. However, by combining this information with details of the internal structure of the lithosphere provided by long-range seismic refraction experiments along isochrons, it may be possible to see whether the thermal structure itself flattens in the way expected for the plate model. In addition to the above observations it should be noted that knowledge of thermal conductivities is critical in many ways to the arguments and calculations of this paper. Repeated measurements to verify the presently accepted values [Fukao et al., 1968; Fukao, 1969; Schatz and Simmons, 1972] and to check the degree of variation possible in the upper mantle would reduce further any uncertainties.

Appendix 1: Solutions of the Corresponding One-Dimensional Heat Flow Problem

Carslaw and Jaeger [1959] comprehensively discuss the solutions of such problems. In particular, they show that if a solution is obtained using the Laplace transform method, then it is possible to give two different forms for the solution by expanding the transform in different ways before inversion. One corresponds to the expansion of the solution as a sine series, the other to an expression in terms of a series of complementary error functions. In the latter the $t^{-\frac{1}{2}}$ structure we are seeking is explicit. Here we demonstrate an alternative approach, using a Green's function method, as this can be compared directly with the Green's function solution to the full equation (3) given in Appendix 2.

The simplest solution to the one-dimensional heat flow equation (6) with the same boundary conditions used in solving (3) has the form

$$T = (1 - x_2) + \sum_{n=1}^{\infty} a_n \exp(-n^2\pi^2 t) \sin n\pi x_2 \quad (24)$$

with $a_n = 2(-1)^{n+1}/n$. Expression (24) obviously corresponds directly to (5), as can be seen by expanding the β_n for $R \gg n$.

To obtain an alternative solution, the expression for the temperature can be written as two parts

$$T = (1 - x_2) + \phi \quad (25)$$

where the first part represents the uniform heat flux background to which the solution decays. The second part satisfies (6), but the boundary conditions become

$$\phi = 0 \quad x_2 = 0,\ x_2 = 1$$
$$\phi = x_2 \quad t = 0 \quad (26)$$

In order to make use of a Green's function in finding a solution with an explicit $t^{-\frac{1}{2}}$ dependence we convert the problem from one confined to the region $0 < x_2 \leq 1$ to one extending over the entire domain $-\infty < x_2 < \infty$. This is done by considering an initial temperature profile for ϕ of the form shown in Figure 14, extending to $\pm\infty$. The temperature distribution is identical to that given by (26) within the range $0 < x_2 < 1$. In the range $-1 < x_2 < 0$ the temperature profile is the negative of that in the principal range, and the remainder of the profile is obtained by repeating this portion with a periodicity of 2 to give a sawtooth pattern. Then the solution for ϕ at any time t may be written down by using the Green's function for (6) in an infinite domain:

$$\phi(x_2, t) = \frac{1}{2(\pi t)^{1/2}} \cdot \int_{-\infty}^{\infty} \phi(x_2', 0) \exp\left[\frac{-(x_2 - x_2')^2}{4t}\right] dx_2' \quad (27)$$

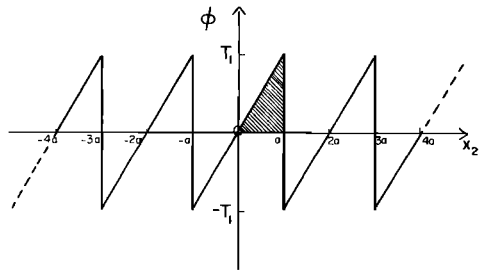

Fig. 14. Initial conditions, in dimensional form, for ϕ extended over an infinite domain to facilitate application of a Green's function method.

[Carslaw and Jaeger, 1959, section 2.2]. The initial distribution shown in Figure 14 is antisymmetric about the points $\pm n$, n = 0, 1, 2, ..., and it is not difficult to show from (27) that $\phi(x_2, t)$ is zero at these points. Hence (27) satisfies (6) and the boundary conditions (26) within the range $0 < x_2 < 1$ and so is the required solution in this range. Substituting for the initial conditions in (27) and making use of the periodicity, we find that

$$\phi(x_2, t) = \sum_{n=-\infty}^{\infty} \frac{1}{2(\pi t)^{1/2}} \tag{28}$$

$$\cdot \int_{-1}^{1} x_2' \exp\left\{\frac{-(x_2 - x_2' - 2n)^2}{4t}\right\} dx_2' \tag{28}$$

After some algebra this expression can be rewritten in the following way:

$$\phi(x_2, t) = x_2 + \sum_{n=0}^{\infty} \left[\operatorname{erfc}\left\{\frac{x_2 + (2n+1)}{2(t)^{1/2}}\right\} - \operatorname{erfc}\left\{\frac{-x_2 + (2n+1)}{2(t)^{1/2}}\right\}\right] \tag{29}$$

This solution has the required form and should be compared with similar solutions obtained by the Laplace transform [Carslaw and Jaeger, 1959, section 12.5]. For small times where $t^{1/2} \ll 1$ most terms can be neglected. The asymptotic expansion of erfc (x) for large x is

$$\operatorname{erfc}(x) \sim \frac{e^{-x^2}}{x(\pi)^{1/2}} \cdot \left[1 + \sum_{m=1}^{\infty} \frac{(-1)^m 1.3, \ldots, (2m-1)}{(2x^2)^m}\right] \tag{30}$$

[Abramowitz and Stegun, 1965], where this expansion has the common property that if the series is truncated, the error is smaller in magnitude than the first term neglected and has the same sign. Hence for $t^{1/2} \ll 1$ in the range $0 < x_2 < 1$, combining (29) with (25), the dominant terms in the series are

$$T \sim 1 - \operatorname{erfc}\left\{\frac{1 - x_2}{2(t)^{1/2}}\right\} = \operatorname{erf}\left\{\frac{1 - x_2}{2(t)^{1/2}}\right\} \tag{31}$$

This is just the solution for the cooling of an infinite half space used by Davis and Lister in their justification of the plots against $t^{1/2}$.

Appendix 2: Alternative Form of the Solution to the Moving Slab Problem

We again use a Green's function method in finding an alternative solution to the full problem. The solution to (3) can be written in the form

$$T = (1 - x_2) + \theta \tag{32}$$

Again, instead of solving for θ in the restricted range $0 < x_2 < 1$ we extend the domain to $-\infty < x_2 < \infty$ and consider the whole of this region to be moving with velocity u to the right. To get a solution with θ zero on the boundaries $x_2 = 0$ and $x_2 = 1$, the boundary condition at $x_1 = 0$ has to be taken to be the sawtooth pattern shown in Figure 14. This solution will then be identical to that required in the range $0 < x_2 < 1$. A Green's function corresponding to (3) has been given by Oldenburg [1975]. Using this, the full solution can be written

$$\theta(x_1, x_2) = \frac{1}{\pi} \int_{-\infty}^{\infty} \theta(0, x_2') \frac{Rx_1 e^{Rx_1}}{[x_1^2 + (x_2 - x_2')^2]^{1/2}} \cdot K_1\left\{R[x_1^2 + (x_2 - x_2')^2]^{1/2}\right\} dx_2' \tag{33}$$

where the Green's function for this problem is

$$G(x_1, x_2) = \frac{1}{\pi} \frac{Rx_1 e^{Rx_1}}{(x_1^2 + x_2^2)^{1/2}} \cdot K_1\left[R(x_1^2 + x_2^2)^{1/2}\right] \tag{34}$$

The function $K_1(z)$ is a modified Bessel function of the first order [Watson, 1966, p. 78]. This solution could be used for numerical purposes for problems not confined to a slab with arbitrary boundary conditions on the vertical boundary. Here we shall be content with showing that an asymptotic expression for (34) is identical to the Green's function used in the one-dimensional approximation. This will give the distance from the vertical boundary where the approximation begins to apply and will provide a formal justification for carrying over the conclusions concerning the $t^{1/2}$ form of the solution. The modified Bessel function has an asymptotic expansion given by:

$$K_\nu(z) \sim \left(\frac{\pi}{2z}\right)^{1/2} e^{-z} \cdot \left[1 + \frac{(4\nu^2 - 1)}{8z} + \frac{(4\nu^2 - 1)(4\nu^2 - 3^2)}{2!(8z)^2} + \ldots.\right] \tag{35}$$

for arg (z) < $3\pi/2$ [Watson, 1966, p. 202]. This expansion again has the asymptotic property that if it is truncated, the series has an error whose magnitude is less than that of the first

neglected term and of the same sign. Hence the first term of (35) is an adequate representation if

$$3/8z \ll 1 \quad \text{or} \quad R(x_1^2 + x_2^2)^{1/2} \gg 3/8 \qquad (36)$$

This is certainly true if $Rx_1 \gg 3/8$. Putting this inequality in terms of dimensional quantities we find that

$$x_1 \gg 3\kappa/4u \qquad (37)$$

is the necessary condition. Assuming the value for κ of 7×10^{-3} cm^2 s^{-1}, the right hand side of (37) can be calculated for different spreading rates, as in Table 7, where the equivalent age is also given. For spreading rates of 1 cm yr^{-1} or greater the first term in (35) is certainly an adequate representation for t greater than 1 m.y. The Green's function then has the approximate form

$$G(x_1, x_2) \sim \frac{1}{(2\pi)^{1/2}} \frac{R^{1/2} x_1}{(x_1^2 + x_2^2)^{3/4}} \cdot \exp\{R[x_1 - (x_1^2 + x_2^2)^{1/2}]\} \qquad (38)$$

This can be simplified one step further. If the inequality

$$(x_2/x_1)^2 \ll 1 \qquad (39)$$

is satisfied in (38), then a further approximation to the Green's function is

$$G(x_1, x_2) \sim \frac{1}{(2\pi)^{1/2}} \frac{R^{1/2}}{x_1^{1/2}} \exp[-(Rx_2^2/2x_1)] \qquad (40)$$

where terms of $O(x_2^2/x_1^2)$ have been neglected. This function has significant values only when

$$Rx_2^2/2x_1 \leqslant 1 \qquad (41)$$

TABLE 7. Values of Distance and Age Equivalent to the Right-Hand Side of Inequality (37)

u, cm yr^{-1}	d, km	t, m.y.
1	1.7	0.17
2	0.83	0.042
3	0.55	0.018
5	0.33	0.007
10	0.17	0.002

A value of $\kappa = 7.10^{-3}$ cm^2 s^{-1} was used.

so that (39) is certainly satisfied if

$$Rx_1 \gg 2 \qquad (42)$$

This is the same type of inequality as given in (37). From Table 7 we see that both inequalities should be safely satisfied when t is greater than 1 m.y. The distance that one must go from the vertical boundary before the approximation is satisfied decreases inversely with the spreading velocity. Recalling the nondimensional form for time, it can be seen that this approximation to the Green's function has exactly the form of the one-dimensional Green's function used in (27). Thus the solutions obtained there are good approximations to the solution (33) when the required inequalities are satisfied. In particular, the form of solution (29) provides an alternative to the original form given by (5).

Acknowledgements. Conversations with Frank Richter in the initial stages of this work were very helpful. Geophysical data acquired by the work of members of Lamont-Doherty Geological Observatory forms a substantial part of the information used in this paper; we would like to thank Phil Rabinowitz, Walter Pitman, and Bill Ludwig for providing us with plots of magnetic anomalies and letting us look at unpublished seismic reflection profiles. We are grateful to Mike Purdy, John Grow, and the IPOD site survey office for enabling us to use the unpublished AII and Digicon profiles. We would like to thank Pam Thompson and Linda Meinke for their help in preparing the figures. This research has been supported by the Office of Naval Research, under grant N0014-75-C-0291, and the National Science Foundation, under grant DES73-00513 A02.

References

Abramowitz, M., and I. A. Stegun (Eds.), Handbook of Mathematical Functions, p. 298, Dover, New York, 1965.

Anderson, R. N., and E. E. Davis, A topographic interpretation of the mathematician ridge, Clipperton Ridge, East Pacific Rise System, Nature, 241, 191-193, 1973.

Anderson, R. N., and J. G. Sclater, Topography and evolution of the East Pacific Rise between 5°S and 20°S, Earth Planet. Sci. Lett., 14, 433-441, 1972.

Berggren, W. A., D. P. McKenzie, J. G. Sclater, and J. E. van Hinte, World-wide correlation of Mesozoic magnetic anomalies and its implications: Discussion, Geol. Soc. Amer. Bull., 86, 267-269, 1975.

Carslaw, H. S., and J. C. Jaeger, Conduction of Heat in Solids, 2nd ed., Oxford University Press, New York, 1959.

Chase, T. E., H. W. Menard, and J. Mammerickx, Bathymetry of the Northern Pacific, charts 1-10, Inst. of Mar. Resour., La Jolla, Calif., 1970.

Christensen, N. I., and M. H. Salisbury, Structure and constitution of the lower oceanic crust, Rev. Geophys. Space Phys., 13, 57-86, 1975.

Davis, E. E., and C. R. B. Lister, Fundamentals of ridge crest topography, Earth Planet. Sci. Lett., 21, 405-413, 1974.

Ewing, M., J. L. Worzel, A. O. Beall, W. A. Berggren, D. Bukry, C. A. Burk, A. G. Fischer,

and E. A. Pessagna, Initial Reports of the Deep Sea Drilling Project, vol. 1, U.S. Government Printing Office, Washington, D.C., 1969.

Ewing, M., G. Carpenter, C. Windisch, and J. Ewing, Sediment distribution in the oceans: The Atlantic, Geol. Soc. Amer. Bull., 84, 71-88, 1973.

Fischer, A. G., B. C. Heezen, R. E. Boyce, D. Bukry, R. G. Douglas, R. E. Garrison, S. A. Kling, V. Krasheninnikev, A. P. Lisitzin, and A. C. Pimm, Initial Reports of the Deep Sea Drilling Project, vol. 6, U.S. Government Printing Office, Washington, D. C., 1971.

Forsyth, D. W., The early structural evolution and anisotropy of the oceanic upper mantle, Geophys. J. Roy. Astron. Soc., 43, 103-162, 1975.

Forsyth, D. W., and F. Press, Geophysical tests of petrological models of the spreading lithosphere, J. Geophys. Res., 76, 7963-7979, 1971.

Fukao, Y., On the radiative heat transfer and the thermal conductivity in the upper mantle, Bull. Earthquake Res. Inst. Tokyo Univ., 47, 549-569, 1969.

Fukao, Y., H. Mizutani, and S. Uyeda, Optical absorption spectra at high temperatures and radiative thermal conductivity of olivines, Phys. Earth Planet. Interiors, 1, 57-62, 1968.

Goranson, R. W., Heat capacity: Heat of fusion, Handbook of Physical Constants, Geol. Soc. Amer. Spec. Pap., 36, 223-242, 1942.

Hayes, D. E., A. C. Pimm, J. P. Beckmann, W. E. Benson, W. H. Berger, P. H. Roth, P. R. Supko, and U. van Rad, Initial Reports of the Deep Sea Drilling Project, vol. 14, U.S. Government Printing Office, Washington, D.C., 1972.

Heezen, B. C., I. D. MacGregor, H. P. Foreman, G. Farristall, H. Hekel, R. Hesse, R. H. Hoskins, E. J. W. Jones, A. G. Kaneps, V. A. Krasheninnikov, H. Okada, and M. H. Ruef, Initial Reports of the Deep Sea Drilling Project, vol. 20, U.S. Government Printing Office, Washington, D.C., 1973.

Heirtzler, J. R., G. O. Dickson, E. M. Herron, W. C. Pitman, and X. LePichon, Marine magnetic anomalies, geomagnetic field reversals, and motions of the ocean floor and continents, J. Geophys. Res., 73, 2119-2136, 1968.

Hess, H. H., History of ocean basins, in Petrologic Studies: A Volume to Honor A.F. Buddington, edited by A.E.J. Engel et al., pp. 599-620, Geological Society of America, New York, 1962.

Hilde, T. W. C., N. Isezaki, and J. M. Wageman, Mesozoic sea floor spreading in the North Pacific, in Geophysics of the Pacific Ocean Basin and its Margin, Geophys. Monogr. 19, edited by G.P. Woollard et al., AGU, Washington, D. C., 1976.

Hollister, C. D., J. I. Ewing, D. Habib, J. C. Hathaway, Y. Lancelot, H. Luterbacher, F. J. Paulus, C. W. Poag, J. A. Wilcoxan, and P. Worstell, Initial Reports of the Deep Sea Drilling Project, vol. 11, U.S. Government Printing Office, Washington, D. C., 1972.

Holmes, A., Radioactivity and earth movements, Trans. Geol. Soc., Glasgow, 18, 559-606, 1931.

Kushiro, I., Y. Syono, and S. Akimata, Melting of a peridotite nodule at high pressures and high water pressures, J. Geophys. Res., 73, 6023-6029, 1968.

Lancelot, Y., and R. L. Larson, Sedimentary and tectonic evolution of the northwestern Pacific, in Initial Reports of the Deep Sea Drilling Project, vol. 32, pp. 925-939, edited by R. L. Larson and R. Moberly et al., U.S. Government Printing Office, Washington, D. C., 1975.

Langseth, M. G., X. LePichon, and M. Ewing, Crustal structure of mid-ocean ridges, 5, Heat flow through the Atlantic Ocean floor and convection currents, J. Geophys. Res., 71, 5321-5355, 1966.

Larson, R. L. and C. G. Chase, Late Mesozoic evolution of the western Pacific Ocean, Geol. Soc. Amer. Bull., 83, 3627-3644, 1972.

Larson, R. L., and T. W. C. Hilde, A revised time scale of magnetic reversals for the early Cretaceous and late Jurassic, J. Geophys. Res., 80, 2586-2594, 1975.

Larson, R. L. and W. C. Pitman, World-wide correlation of Mesozoic magnetic anomalies, and its implications, Geol. Soc. Amer. Bull., 83, 3645-3662, 1972.

Larson, R. L., and W. C. Pitman, World-wide correlation of Mesozoic magnetic anomalies and its implications: Reply, Geol. Soc. Amer. Bull. 86, 270-272, 1975.

Larson, R. L., R. Moberly, D. Bukry, H. P. Foreman, J. V. Gardner, J. B. Keene, Y. Lancelot, H. Luterbacher, M. C. Marshall, and A. Matter, Initial Reports of the Deep Sea Drilling Project, vol. 32, U.S. Government Printing Office, Washington, D. C., 1975.

Laughton, A. S., W. A. Berggren, R. N. Benson, T. A. Davies, U. Franz, L. F. Musich, K. Perch-Nielsen, A. S. Ruffman, J. E. van Hinte, and R. B. Whitmarsh, Initial Reports of the Deep Sea Drilling Project, vol. 12, U.S. Government Printing Office, Washington, D. C., 1972.

Leeds, A. R., L. Knopoff, and E. G. Kausel, Variations of upper mantle structure under the Pacific Ocean, Science, 186, 141-143, 1974.

Lister, C. R. B., On the thermal balance of a mid-ocean ridge, Geophys. J. Roy. Astron. Soc., 26, 515-535, 1972.

Lister, C. R. B., On the penetration of water into hot rock, Geophys. J. Roy. Astron. Soc., 39, 465-509, 1974.

Lister, C. R. B., Estimators for heat flow and deep rock properties, based on boundary layer theory, paper presented at the Sixteenth General Assembly, Int. Union of Geod. and Geophys., Grenoble, France, 1975.

Lubimova, E. A., and V. N. Nikitina, On heat flow singularities over mid-ocean ridges, J. Geophys. Res., 80, 232-243, 1975.

Matthews, D. J., Tables of the velocity of sound in pure water and seawater for use in echo-sounding and sound-ranging, H.D. 282, 52 pp., Hydrogr. Dep., Admiralty, London, 1939.

McKenzie, D. P., Some remarks on heat flow and gravity anomalies, J. Geophys. Res., 72, 6261-6273, 1967.

McKenzie, D. P. and J. G. Sclater, Heat flow in the eastern Pacific and sea-floor spreading, Bull. Volcanol., 33, 101-118, 1969.

McKenzie, D. P., and J. G. Sclater, The evolution of the Indian Ocean since the Cretaceous,

Geophys. J. Roy. Astron. Soc., 24, 437-509, 1971.
McKenzie, D., and C. Bowin, The relationship between bathymetry and gravity in the Atlantic Ocean, J. Geophys. Res., 81, 1903-1915, 1976.
McKenzie, D., and N. Weiss, Speculations on the thermal and tectonic history of the earth, Geophys. J. Roy. Astron. Soc., 42, 131-174, 1975.
Morgan, W. J., Heat flow and vertical movements of the crust, in Petroleum and Global Tectonics, edited by A. G. Fischer and S. Judson, Princeton University Press, Princeton, N. J., 1975.
Oldenburg, D. W., A physical model for the creation of the lithosphere, Geophys. J. Roy. Astron. Soc., 43, 425-451, 1975.
Parker, R. L., and D. W. Oldenburg, Thermal model of ocean ridges, Nature Phys. Sci., 242, 137-139, 1973.
Peterson, M. N. A., N. T. Edgar, M. Cita, S. Gartner, R. Goll, C. Nigrini, and C. von der Borch, Initial Reports of the Deep Sea Drilling Project, vol. 2, U.S. Government Printing Office, Washington, D. C., 1970.
Pitman, W. C., and M. Talwani, Sea-floor spreading in the North Atlantic, Geol. Soc. Amer. Bull., 83, 619-646, 1972.
Richter, F. M., Convection and the large-scale circulation of the mantle, J. Geophys. Res., 78, 8735-8745, 1973.
Richter, F. M., and B. Parsons, On the interaction of two scales of convection in the mantle, J. Geophys. Res., 80, 2529-2541, 1975.
Schatz, J. F., and G. Simmons, Thermal conductivity of earth materials at high temperatures, J. Geophys. Res., 77, 6966-6983, 1972
Scientific Staff, Deep Sea Drilling Project, Leg 37, Geotimes, 19, 16-18, 1974.
Scientific Staff, Deep Sea Drilling Project, Leg 41, Geotimes, 20, 18-21, 1975.
Sclater, J. G., and R. Detrick, Elevation of mid-ocean ridges and the basement age of Joides deep sea drilling sites, Geol. Soc. Amer. Bull., 84, 1547-1554, 1973.
Sclater, J. G., and J. Francheteau, The implications of terrestrial heat flow observations on current tectonic and geochemical models of the crust and upper mantle of the earth, Geophys. J. Roy. Astron. Soc., 20, 509-542, 1970.
Sclater, J. G., R. N. Anderson, and M. L. Bell, Elevation of ridges and evolution of the central eastern Pacific, J. Geophys. Res., 76 7888-7915, 1971.
Sclater, J. G., L. A. Lawver, and B. Parsons, Comparisons of long wavelength residual elevation and free air gravity anomalies in the North Atlantic and possible implications for the thickness of the lithospheric plate, J. Geophys. Res., 80, 1031-1052, 1975.
Sclater, J. G., J. Crowe, and R. N. Anderson, On the reliability of oceanic heat flow averages, J. Geophys. Res., 81, 2997-3006, 1976.
Skinner, B. J., Thermal expansion, Handbook of Physical Constants, Geol. Soc. Amer. Mem., 97, 75-96, 1966.
Sleep, N. H., Sensitivity of heat flow and gravity to the mechanism of sea-floor spreading, J. Geophys. Res., 74, 542-549, 1969.
Solomon, S. C., Shear wave attenuation and melting beneath the mid-Atlantic Ridge, J. Geophys. Res., 78, 6044-6059, 1973.
Sorokhtin, O. G., Dependence of the topography of mid-ocean ridges on the rate of spreading of the ocean floor (in Russian), Dokl. Akad. Nauk SSSR, 208, 1338-1341, 1973.
Talwani, M. (General Ed.), Lamont-Doherty Survey of the World Ocean, Underway Marine Geophysical Data in the North Atlantic, June 1961-January 1971, Lamont-Doherty Geological Observatory, Columbia University, Palisades, N. Y., 1974.
Talwani, M., C. C. Windisch, and M. G. Langseth, Reykjanes ridge crest: A detailed geophysical study, J. Geophys. Res., 76, 473-517, 1971.
Trehu, A., J. G. Sclater, and J. Nabelek, The depth and thickness of the ocean crust and its dependence upon age, Bull. Soc. Geol. Fr., in press, 1976.
Turcotte, D. L., and E. R. Oxburgh, Finite amplitude convective cells and continental drift, J. Fluid Mech., 28, 29-42, 1967.
Uchupi, E., Bathymetric atlas of the Atlantic, Caribbean, and Gulf of Mexico, Rep. 71-72, Woods Hole Oceanogr. Inst., Woods Hole, Mass., 1971.
van Hinte, J. E., A Jurassic time scale, Amer. Ass. Petrol. Geol. Bull., 60, 489-497, 1976.
Vogt, P. R., and N. A. Ostenso, Steady state crustal spreading, Nature, 215, 811-817, 1967.
Vogt, P. R., C. N. Anderson, and D. R. Bracey, Mesozoic magnetic anomalies, sea floor spreading and geomagnetic reversals in the southwestern North Atlantic, J. Geophys. Res., 76, 4796-4823, 1971.
Watson, G. N., A Treatise on the Theory of Bessel Functions, 2nd, ed., Cambridge University Press, New York, 1966.
Watts, A. B., Gravity and bathymetry in the Central Pacific Ocean, J. Geophys. Res., 81, 1533-1553, 1976.
Williams, D. L., R. P. von Herzen, J. G. Sclater, and R. N. Anderson, The Galapagos spreading centre: Lithospheric cooling and hydrothermal circulation, Geophys. J. Roy. Astron. Soc., 38, 587-608, 1974.
Winterer, E. L., W. R. Riedel, P. Brönnimann, E. L. Gealy, G. R. Heath, L. Kroenke, E. Martini, R. Moberly, Jr., J. Resig, and T. Worsley, Initial Reports of the Deep Sea Drilling Project, vol. 7, U.S. Government Printing Office, Washington, D. C., 1971.
Winterer, E. L., J. I. Ewing, R. G. Douglas, R. D. Jarrard, Y. Lancelot, R. M. Moberly, T. C. Moore, Jr., P. H. Roth, and S. O. Schlanger, Initial Reports of the Deep Sea Drilling Project, vol. 17, U.S. Government Printing Office, Washington, D. C., 1973.
Woollard, G. P., The interrelationships of crustal and upper mantle parameter values in the Pacific, Rev. Geophys. Space Phys., 13, 87-137, 1975.
Wyllie, P. J., The Dynamic Earth: Textbook in Geosciences, chap. 8, John Wiley, New York, 1971.

(Received February 17, 1976;
revised July 8, 1976;
accepted July 19, 1976.)